

Carbon dioxide exchange fluxes of a boreal peatland over a complete growing season, Komi Republic, NW Russia

Julia Schneider · Lars Kutzbach ·
Martin Wilming

Received: 8 July 2010 / Accepted: 18 November 2011 / Published online: 30 November 2011
© Springer Science+Business Media B.V. 2011

Abstract The carbon pool of peatlands has been considered as potentially unstable in a changing climate. This study is the first presenting carbon dioxide (CO₂) net ecosystem exchange, CO₂ efflux due to ecosystem respiration and CO₂ uptake by gross primary production over a complete growing season for different microforms of a boreal peatland in Russia (61°56'N, 50°13'E). CO₂ fluxes were measured using the closed chamber technique from the 25th April in the period of snow melt until the end of the vegetation period and the first frost on the 20th October 2008 at seven different microform types: minerogenous and ombrogenous hollows, lawns and hummocks, respectively, and *Carex* lawns situated in a transition zone between minerogenous and ombrogenous mire parts. The total number of chamber flux measurements was 5,517. Ombrogenous hummocks and lawns were sources of CO₂ over the investigation period whereas hollows and minerogenous lawns were CO₂ sinks. Some plots of *Carex* lawns and minerogenous hummocks were sinks while other plots of these microform types were sources. The CO₂ fluxes were characterised by large variability not only between the

microform types but also within the respective microform types. Of all microform types, the *Carex*, ombrogenous, and minerogenous lawns showed the highest variability in CO₂ fluxes, which is probably related to a stronger within-microform heterogeneity in vegetation composition and coverage as well as in the water table level. Air temperature was one of the dominant controls on the CO₂ flux dynamics. Water table and green area index were found to have strong influence on CO₂ fluxes both within different patches of the same microform type as well as between different microforms.

Keywords CO₂ · Net ecosystem exchange · Photosynthesis · Respiration · Boreal peatland ecosystem · Microform · Vegetation composition · Water table · Leaf area index · Spatial variation · Russia

Introduction

Peatlands are well known to be a long-term sink for atmospheric carbon dioxide (CO₂), but the CO₂ fluxes could be substantially altered in a changing climate, and peatlands may become a source of atmospheric carbon (Gorham 1991; Schreder et al. 1998; Aurela et al. 2002). Recently, boreal peatlands have been subject to many speculations regarding climate change effects and greenhouse gas exchange. Some boreal peatlands were shown to be sinks of atmospheric CO₂ (Shurpali et al. 1995; Alm et al. 1999;

J. Schneider (✉) · M. Wilming
Institute of Botany and Landscape Ecology,
Ernst Moritz Arndt University Greifswald, Grimmer
Straße 88, 17487 Greifswald, Germany
e-mail: schneider.jul@web.de

L. Kutzbach
Institute of Soil Science, KlimaCampus, University of
Hamburg, Allende-Platz 2, 20146 Hamburg, Germany

Sagerfors et al. 2008); whereas others were shown to be sources (Shurpali et al. 1995; Alm et al. 1999; Waddington and Roulet 2000). Many studies on CO₂ fluxes have been conducted in the boreal zone of North America (e.g. Schreuder et al. 1998; Moore et al. 2002) and Scandinavia (Alm et al. 1997; Waddington and Roulet 1996; Lindroth et al. 2007; Riutta et al. 2007a; Sagerfors et al. 2008) and in the Russian tundra (Heikkinen et al. 2004; Zamolodchikov et al. 2003; van der Molen et al. 2007; Kutzbach et al. 2007a), but hardly any in boreal Russia. The Russian boreal zone covers vast areas, and peatlands are one of the major ecosystems of this region. Estimations by Apps et al. (1993) showed that 136 Mha of boreal Russia are covered by peatlands and about 50% of the world's boreal peatlands are located in Russia. The carbon sink strength of the Siberian peatlands is probably comparable to those of old pine forests (Valentini et al. 2000). However, still little scientific evidence based on measurements is available from peatland ecosystems of this region. The CO₂ dynamics of peatlands of the boreal zone of Siberia were studied by Panikov and Dedysh (2000), Arneth et al. (2002) and Schulze et al. (2002). Their results describe a significant net carbon uptake of boreal bogs during years with average climatic conditions. Nevertheless, the carbon fixation was higher in cool and wet years compared to dry and warm years when a bog may become a source of atmospheric carbon.

The main objectives of this study were: (1) to investigate the seasonal dynamics of the CO₂ fluxes at various microforms of a boreal peatland in the rarely investigated European part of northern Russia (61°56'N, 50°13'E) and (2) to identify the principal environmental control mechanisms of the CO₂ exchange between the peatland and the atmosphere. The collected data were used (3) to calculate an annual budget of the CO₂ fluxes for the investigation area and (4) to compare the results of two different methods for modelling CO₂ net ecosystem exchange.

Methods

Study site

The study site is the boreal peatland complex Ust-Pojeg (61°56'N, 50°13'E) and is located in east European Russia northwest of Syktyvkar, the capital

of the Komi Republic (Fig. 1), and about 1,000 km northeast from Moscow. The climate is boreal continental and all-year humid with maximum precipitation in summer. The Syktyvkar meteorological station (61°40'N, 50°51'E) is the nearest (45 km) long-term meteorological station to the Ust-Pojeg peatland. The long-term mean annual precipitation is 465 mm, and mean annual temperature is 1.9°C (1999–2008), ranging from monthly averages of –12.7°C in January to 18.2°C in July. The long-term average length of the growing season (period when the mean daily temperature exceeds 5°C) is 157 days (RWS 2009). Figure 2 presents the monthly mean temperatures (A) and monthly precipitation sums (B) for the investigation period in 2008 at the investigation site Ust-Pojeg and in Syktyvkar, and the long-term averages for the period of 1999–2008 in Syktyvkar.

The Ust-Pojeg peatland is composed of ombrogenous bog areas and minerogenous, though oligotrophic, fen areas. Within the peatland, we defined an intensive study area which was a circular area with a diameter of 600 m with a meteorological station placed in the centre. The intensive study site area was comprised of a *Sphagnum angustifolium* pine bog in its northern part and a *Sphagnum jensenii* fen in its southern part. The pH in the peat pore water is about 4 in the bog part and 5 in the fen part (Wolf 2009). Both the northern bog part and the southern fen part of the study area at the Ust-Pojeg peatland are composed of a mosaic of different microforms defined by their situation within the microrelief. Hummocks which represent the driest conditions are elevated above the surrounding area and are covered by *Andromeda polifolia*, *Chamaedaphne calyculata*, *Betula nana* and *Pinus sylvestris*. The hollows represent the wettest microforms and are occupied primarily by *Scheuchzeria palustris* and *Carex limosa*. The vegetation of lawns, intermediate microforms with respect to water level, consists of a mixture of species growing at hummocks and hollows. The differences in the nutrient conditions of the fen and bog part are indicated by the occurrence of *Menyanthes trifoliata* and *Utricularia intermedia* in the fen part of the investigation area. The transition zone between the fen and bog part is characterised by *Carex rostrata* lawns and ombrogenous lawns. A detailed description of the vegetation characteristics and water table depth is given in the Appendix (see Table 4). Average peat depth is about 2 m.

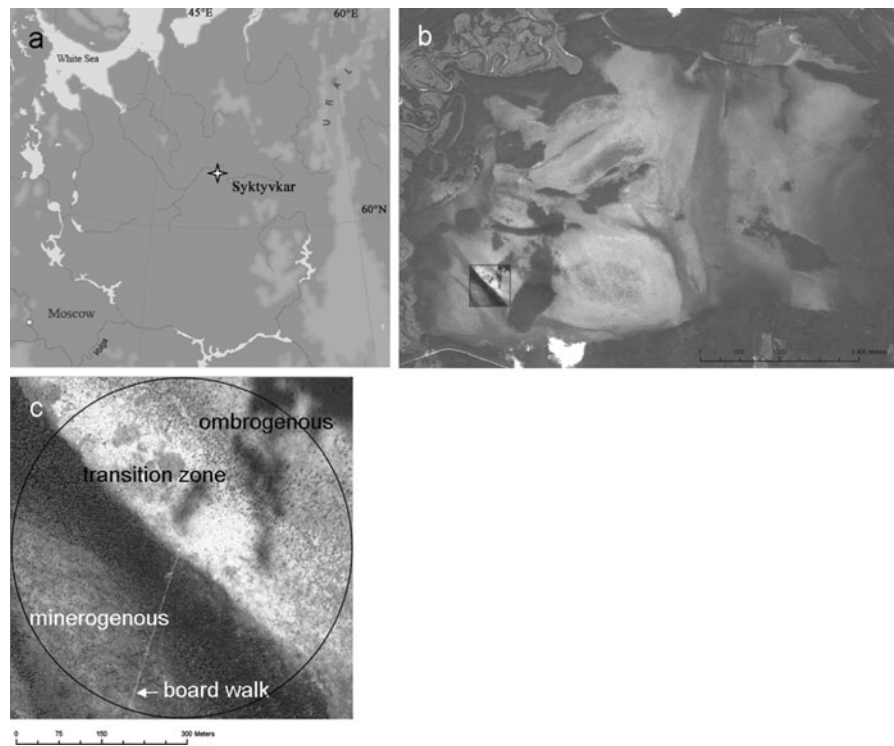


Fig. 1 **a** Map of European Russia. The study was conducted 45 km NW of Syktyvkar. **b** Ust-Pojeg peatland study site. **c** More detailed view on the study site. Area inside the circle

indicates the intensive study site. Original data for **b** and **c** by QuickBird® DigitalGlobe™, distributed by Eurimage/Pöyry Environment Oy

Experimental setup

CO₂ exchange was measured four times per week from 23rd April to 20th October 2008 applying a closed chamber approach. To capture the diurnal variation in CO₂ fluxes, we conducted series of measurements once per week during morning (5 am to 11 am local time) and once per week during evening (6 pm to 12 pm local time); the two other series of measurements were conducted during daytime. In total, 5,517 closed-chamber measurements were performed.

18 measurement plots were established within the intensive study site at different microform types: 2 replicates each in ombrogenous hollows (OHO), lawns (OL) and hummocks (OH), and 3 replicates each in minerogenous hollows (MHO), lawns (ML) and hummocks (MH), and *Carex rostrata* lawns (CL). The sample plots were chosen subjectively, after a visual inspection of the site considering vegetation composition and position in the microrelief. The arrangement of the measurement plots had to satisfy different goals: to cover the spatial variation in

vegetation and water table levels and to be as close as possible to each other because heavy, bulky equipment was used for the measurements. At each measurement plot, a permanent collar was installed at least two weeks before the start of the chamber measurements. The insertion depth of the collars was 15–40 cm, depending on the average water table depth. Elevated boardwalks were built to prevent disturbance of the plant cover and peat during the measurements. The soil temperature was measured at depths of 5, 10, 20 and 40 cm with sampling intervals of 30 min (HOBO U12, HOBO, USA). In the ombrogenous part of the peatland, each sampling plot was equipped with a soil temperature logger, in the transition zone one logger was installed and in the minerogenous part two loggers per microform type were installed. The depth of ground water near the collars was measured manually on each sampling day at each measurement plot, with one exception: plots 7 and 8 shared one well. The measurement was conducted using the bubble tube. The length of the plastic tubing was marked in centimetres and lowered

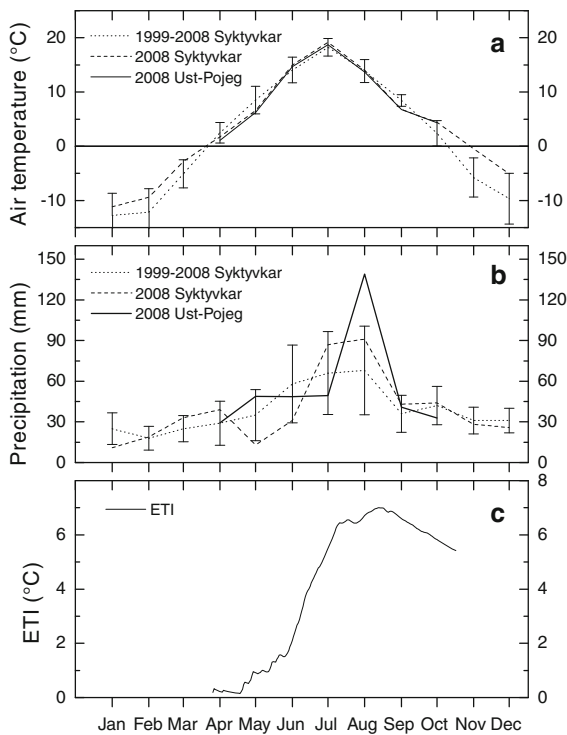


Fig. 2 **a** Monthly mean temperatures at Ust-Pojeg study site in 2008 and at Syktyvkar meteorological station in 2008 and for the period 1999–2008. **b** Monthly mean precipitation at Ust-Pojeg study site in 2008 and at Syktyvkar meteorological station in 2008 and for the period 1999–2008. *Error bars* indicate standard deviations for the long term monthly mean temperature and precipitation. **c** Effective temperature index (ETI) for 2008 at Ust-Pojeg peatland (see Eq. 1 and the text for explanation)

down the well during the measurement. Contact with the standing water is distinguished by blowing into the tube and listening for the sound of bubbles. Photosynthetically active radiation (PAR) was measured with a quantum sensor (SKP215, Skye Instruments Ltd., UK) and the air temperature with a temperature probe (CS 215, Campbell Scientific, USA) at the weather station in Ust-Pojeg peatland at a height of 2 m above the ground. Friction velocity (u_*) was used to describe atmospheric turbulence conditions and was calculated over half-hour intervals from 20 Hz wind vector measurements by a three-dimensional sonic anemometer at 3 m above the ground (Gill 3R, Gill Instr., UK).

The green leaf area index (GAI) was determined to describe the vegetation development over the growing season. The method was thoroughly described by Wilson et al. (2007). The green leaf area index of vascular plants (GAI_{vasc}) was calculated as a product

of the leaf size and number of green leaves in plots of dimensions 60×60 cm every 2 weeks. The number of the leaves of each species in each plot was counted. If the vegetation was very dense, five permanent sub-samples (10×10 cm) in each plot were marked, and the leaves were counted only in for these sub-plots. Species which show large seasonal dynamics in leaf size, e.g. sedges, were measured non-destructively with a tape measure on five marked shoots outside of the plots. Species which have a relatively stable leaf size during the whole growing season, e.g. shrubs, were measured only once during summer. The seasonal development of GAI_{vasc} was unimodal and approximately Gaussian-like-distributed with clearly defined maxima. For modelling of the GAI_{vasc} over the season, we fitted a Gaussian-type function to the measured data. The green leaf area of mosses (GAI_{moss}) was estimated as the projection coverage of living moss capitula which was about $0.75 \text{ m}^2 \text{ m}^{-2}$. This estimated moss cover was assumed to be constant over the growing season. GAI was calculated as a sum of GAI_{vasc} and GAI_{moss} and was used as an explanatory variable for modelling the CO_2 fluxes.

The effective temperature sum index (ETI) was used to describe the thermal characteristics of the investigated area and was calculated by dividing the cumulative effective temperature sum by the number of days (d) counted from 1st of April as follows (Alm et al. 1997, 1999):

$$ETI(d) = \frac{\sum_{i=1}^d (T_i - T_t)}{d} \quad (1)$$

where, T_i is the mean daily air temperature on day number i , and T_t is the daily mean temperature threshold of 5°C .

CO_2 flux measurements

The closed chamber technique was applied to determine the CO_2 net ecosystem exchange (NEE), the CO_2 efflux due to ecosystem respiration (R_{eco}) and the CO_2 uptake by gross primary production (GPP). NEE was measured using a transparent chamber ($60 \times 60 \times 32$ cm) made of polycarbonate sheets with a thickness of 1.5 mm. For R_{eco} measurements, the chamber was covered with an aluminium shroud. The chamber was equipped with a fan, and the headspace air temperature was controlled to within approximately $\pm 1^\circ\text{C}$ of the

ambient temperature by an automatic cooling system using ice water as coolant. A PAR sensor (SKP212, Skye Instruments Ltd., UK) was installed inside the chamber. During the flux measurements, the chamber was put on the preinstalled collars, which were equipped with a water-filled groove around the top to avoid air exchange between the headspace and the ambient air. Initial pressure shocks during the chamber setting were minimised by two large openings on top of the chamber which were closed only after setting the chamber. The CO₂ concentrations were measured using a CO₂/H₂O infrared gas analyzer (LI-840, Licor, USA). CO₂ readings were taken at 1 s intervals over 180 s. The data was recorded using a data logger (CR850, Campbell Scientific, USA). The CO₂ flux was calculated from the change in CO₂ concentration in the chamber headspace by fitting an exponential model and determining the rate of initial concentration change at the start of the closure period. More detailed information about the fit method can be found in Kutzbach et al. (2007b). If the curvature of the nonlinear curves was not explainable by the theoretical model presented in Kutzbach et al. (2007b), the slope of a linear regression line was used for estimating the flux.

Screening and modelling of CO₂ fluxes

It was shown previously that measurements of CO₂ fluxes by the closed chamber method can be disturbed during low atmospheric turbulence conditions (Schneider et al. 2009). In order to exclude data disturbed by low atmospheric turbulence from further analyses, we used a friction velocity threshold of 0.1 m s⁻¹ for screening the data. For modelling of the seasonal CO₂ fluxes 265 measurements conducted during calm night conditions ($u_* < 0.1 \text{ m s}^{-1}$, $\text{PAR} \leq 10 \text{ } \mu\text{mol m}^{-2}\text{s}^{-1}$) were rejected.

For modelling of CO₂ fluxes, models based on photosynthetically active radiation (PAR in $\mu\text{mol m}^{-2}\text{s}^{-1}$), air temperature (T in °C), water table depth (WT in cm) and GAI (in $\text{m}^2 \text{ m}^{-2}$) or ETI as explanatory variables were used. To analyse the differences between microform types but also between different plots of one microform type, each measurement plot was modelled separately. The data sets of individual sample plots were large enough to obtain

acceptable models. NEE was empirically modelled using the following functional forms:

$$\begin{aligned} \text{NEE} &= \text{GPP} + R_{\text{eco}} \\ &= \frac{P_1 \times \text{GAI} \times \text{PAR}}{\text{PAR} + k_1} + a_1 \times \exp(b_1 \times T) \\ &\quad \times \exp(c_1 \times \text{WT}) \end{aligned} \quad (2)$$

or

$$\begin{aligned} \text{NEE} &= \text{GPP} + R_{\text{eco}} \\ &= \frac{P_1 \times \text{ETI} \times \text{PAR}}{\text{PAR} + k_1} + a_1 \times \exp(b_1 \times T) \\ &\quad \times \exp(c_1 \times \text{WT}). \end{aligned} \quad (3)$$

Furthermore, we performed a separate modelling of R_{eco} and gross primary production (GPP). R_{eco} fluxes were related to air temperature and water tables following Larmola et al. (2004):

$$R_{\text{eco}} = a_2 \times \exp(b_2 \times T) / (1 + \exp(-(WT - u)/s)) \quad (4)$$

or following Alm et al. (1997) when the data range was not appropriate for fitting Eq. 4:

$$R_{\text{eco}} = a_2 \times \exp(b_2 \times T) \times \exp(c_2 \times \text{WT}). \quad (5)$$

For an estimate of GPP, values of measured R_{eco} fluxes were subtracted from values of measured NEE fluxes measured directly before the R_{eco} measurement. These estimated values for GPP were used for modelling GPP over the investigation period using the modified rectangular hyperbola function introduced by Kettunen (2000):

$$\text{GPP} = \frac{P_2 \times T \times \text{GAI} \times \text{PAR}}{\text{PAR} + k_2} \quad (6)$$

or

$$\text{GPP} = \frac{P_2 \times T \times \text{ETI} \times \text{PAR}}{\text{PAR} + k_2} \quad (7)$$

where, P_1 , k_1 , a_1 , b_2 , c_1 , a_2 , b_2 , c_2 , u , s , P_2 and k_2 are fitting parameters.

In this study, NEE is defined negative when the absolute value of GPP exceeds the absolute value of R_{eco} and there is a net removal of carbon dioxide from the atmosphere. NEE is defined positive when the absolute value of R_{eco} exceeds the absolute value of GPP and carbon dioxide is released to the atmosphere. Hence, GPP and carbon dioxide uptake were defined

as a negative flux and R_{eco} and carbon release to the atmosphere as a positive flux.

The reduction of radiation by chamber walls was assessed from measurements of PAR inside and outside the chamber (Fig. 3). PAR inside the chamber (mean of the first ten seconds of the measurement) is on average 30% lower than the mean PAR value measured at the weather station over the respective half-hour measurement interval. The difference between PAR measured inside and outside the chamber was highly variable depending on sun elevation and cloud cover. A reduction of the PAR inside the chamber causes lower photosynthetic rates inside the chamber than outside. The modelling of the seasonal time series of NEE and GPP not disturbed by a chamber was a two-step procedure which involves the derivation of the model parameters using the PAR measured in the chamber during the employment of the chamber and the modelling of NEE and GPP time series over the growing season using the derived model parameters and the half-hourly mean PAR values measured at the weather station as input variables.

PAR variation during the chamber employment period can have disturbing effects on the CO_2 concentration-over-time curves which were used for the flux calculation. As such strongly disturbed concentration-over-time curves show pronounced autocorrelation of the residuals of the exponential fit function, these disturbed chamber experiments were filtered out using

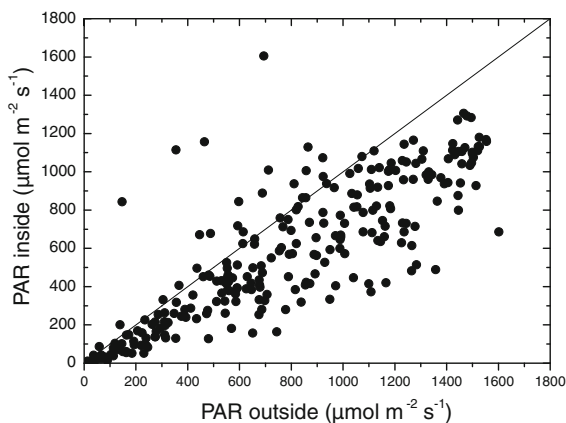


Fig. 3 Comparison of photosynthetically active radiation (PAR) inside and outside of the chamber. PAR inside the chamber is the mean of the first ten seconds of the flux calculation period, PAR outside the chamber is the half-hourly mean for the according half hour measured at the weather station. The 1:1 line indicating a perfect match is shown

a threshold for residual autocorrelation as indicated by the Durbin–Watson test (dL).

NEE, R_{eco} and GPP fluxes were modelled over the complete investigation period to investigate the principal environmental control mechanisms of the CO_2 exchange. To test whether the NEE results depend on the approach used for the estimation, we compared two methods of modelling the NEE time series: (1) by applying the empirical models derived from fitting Eq. 2 or 3 directly to the NEE measurement data and (2) by calculating the NEE time series from the sums of the modelled values of R_{eco} and GPP derived from fitting Eqs. 4 and 5 to the R_{eco} measurements and Eqs. 6 and 7 to the GPP estimates, respectively. Empirical modelling was conducted by nonlinear least-squares fitting using the function *nlinfit* of the MATLAB[®] software package (version 7.1, The MathWorks Inc., Natick, USA).

To compare the results of different NEE estimation methods, we compared the measured NEE fluxes (NEE_{meas}) and NEE fluxes derived by the two models ($\text{NEE}_{\text{mod-1}}$, $\text{NEE}_{\text{mod-2}}$) using the Willmott index of agreement, d_w (Willmott 1982; Yurova et al. 2007).

$$d_w = 1 - \left[\frac{\sum_{i=1}^N (M_i - O_i)^2}{\sum_{i=1}^N (|M'_i| + |O'_i|)^2} \right], \quad (8)$$

where, $M'_i = M_i - \bar{O}$, $O'_i = O_i - \bar{O}$, M —modeled values ($\text{NEE}_{\text{mod-1}}$ or $\text{NEE}_{\text{mod-2}}$) and O —observed values (NEE_{meas}). \bar{O} is the mean of observed values. The Willmott index d_w varies between 0 and 1, with $d_w = 1$ indicating a perfect match.

For calculating the intensive study site's overall CO_2 balance, the relative cover of the different microform types was determined along eight transects. The method was described by Laine et al. (2006). All 300 m long transects started at the centre point of the investigation area and headed toward the cardinal and intercardinal directions. The contributions of the microform types along each transect were recorded, and the percentage contribution was assumed to be representative for the spatial coverage of the microform types in the surrounding 45° sector. Each sector was defined as 1/8 of the intensive study site's circular area and included the transect in the middle of the sector.

The error of the area estimates for the different microforms cannot be considered as random error. Thus, the error propagation routine for random errors is not suitable for the uncertainty analysis of the

upscaled CO₂ fluxes, and we used the method of maximum error estimation.

In order to estimate the uncertainty of the upscaled fluxes (δF), we used the formula:

$$\delta F = \sum_{i=1}^N A_i \times \delta F_i + |F_i| \times \delta A_i, \quad (9)$$

where, F_i is the mean NEE flux of the different microform types and δF_i is the uncertainty of the mean NEE flux. A_i is the mean relative coverage of the different microform types within the area of interest and δA_i is the uncertainty of the coverage estimation.

Results

Weather, soil conditions and vegetation development during the investigation period

At the beginning of the investigation period, the daily average air temperature did not exceed 2°C (Fig. 2). The thermal growing season (mean daily temperature of five consecutive days exceeding 5°C) started on the 25th May and continued until 7th October. The length of the growing season 2008 was accordingly 154 days. The highest mean daily temperatures (25–31°C) were recorded between 21st and 26th June and 18th and 23rd July. Cold (10–15°C) and rainy periods of two to five days followed the warm periods. During the summer, night temperatures frequently fell below 10°C, and occasionally below 5°C. After the 7th September the daily mean air temperature did not exceed 10°C and dropped below 0°C around the 15th October. The monthly air temperatures in 2008 slightly differed from the ten-year average with colder April, May and September and a warmer October (Fig. 2).

At the start of the measuring campaign, the investigation area was no longer snow-covered although some precipitation still fell as snow. Underground ice was present until around the 29th April. August was exceptionally wet; the precipitation was nearly as high as the sum of the preceding three months (149 mm) (Fig. 2). In October, some snow showers passed, but the snow cover did not remain longer than one day.

Precipitation, evapotranspiration and lateral flow of ground water kept the water table in continuous

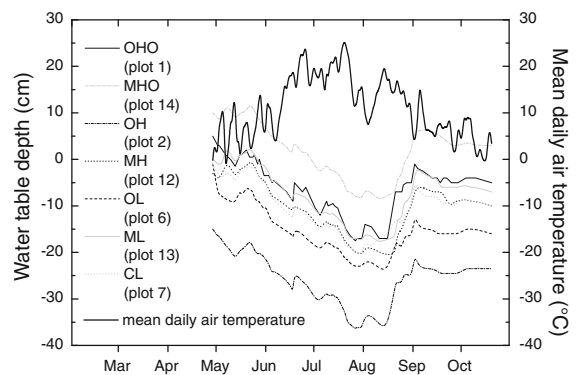


Fig. 4 Mean daily air temperature and water table depth of different microform types in Ust-Pojeg peatland: ombrogenous hollows (OHO), lawns (OL) and hummocks (OH), and minerogenous hollows (MHO), lawns (ML) and hummocks (MH), and *Carex rostrata* lawns (CL). Each microform type is illustrated by one measurement plot as example

change (Fig. 4). The temporal range of water table at the individual measurement plots was 19–23 cm. The average, maximum and minimum water table depths are shown in Table 4 in appendix.

The seasonal development of the effective temperature index is shown in Fig. 2c. ETI started to increase slowly in April followed by steep increase in May and June. The highest ETI values could be observed in August followed by a slow decrease in September and October.

The GAI development varied strongly between the microforms; an earlier increase of GAI in spring was observed at hummock sites compared to hollow sites but the hollows were characterised by a steeper increase in GAI in spring than the hummocks and lawns (Fig. 5). At all sites, the GAI reached its maximum in August, but the maximum values varied considerably. Highest maximum GAI values (3.5 m² m⁻²) occurred at minerogenous hollow sites; lowest GAI values (0.3 m² m⁻²) occurred at ombrogenous hummock sites (Table 4 in appendix).

Measured CO₂ fluxes

The highest maximum values of CO₂ net uptake were measured at minerogenous lawns, followed by *Carex* lawns, minerogenous hummocks and hollows (Fig. 6). Microforms in the ombrogenous part of the peatland were characterised by lower maximum values of CO₂ net uptake than in the minerogenous part. The highest maximum values of CO₂ net release were found at

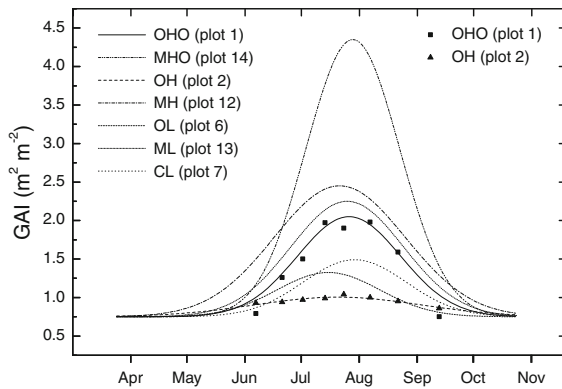


Fig. 5 Modelled green leaf area index (*lines*) of vascular plants for different microform types. Microform acronyms are explained in Fig. 4 and the text. Each microform type is represented by one plot as example. *Squares* and *triangles* represent examples for discrete measured GAI of vascular plants for ombrogenous hollows and ombrogenous hummocks, respectively

Carex lawn sites, followed by minerogenous and ombrogenous hummocks, while the lowest maximum values of CO_2 net release were observed at minerogenous hollow sites.

Seasonal patterns of NEE were well expressed at all microforms; however, they considerably differed between microform types (Fig. 6). At hollow sites, daytime R_{eco} exceeded the photosynthetic activity until around 6th June resulting in net CO_2 release even during the day. Hummocks behaved differently: the photosynthetic activity was higher than daytime respiration from the beginning of the measurement period resulting in CO_2 net uptake during the daytime. CO_2 net uptake increased to its maximum between 23rd July and 10th August, following the seasonal GAI development. From the 5th September, the daytime respiration again continuously exceeded the photosynthetic activity at hollow sites. The vegetation at hummock sites and at *Carex* lawns continued to have higher photosynthetic activity than the respiration during the day until the end of the measurement period.

Clear differences in daytime R_{eco} were found between the microform types. The highest maximum R_{eco} fluxes during the day were observed at minerogenous hummocks and ombrogenous lawns, followed by *Carex* lawns and ombrogenous hummocks (Fig. 7). Highest R_{eco} fluxes occurred at all microforms in July and August. At all microforms except hummocks, the respiration rates were higher in autumn (September–October) than in spring (April–May). The highest

maximum GPP values were observed at minerogenous lawns, followed by *Carex* lawns and minerogenous hummocks (Fig. 8). In general, minerogenous microform types had higher GPP than the analogous ombrogenous microform types. The annual peak in GPP occurred at all microforms during July and August.

Environmental controls on NEE, R_{eco} and GPP and modelling the carbon balance

Air temperature was one of the dominant controls on NEE dynamics. A model composed of an air temperature- and GAI-dependent light saturation function and an exponential function to reflect the dependency of R_{eco} on air temperature was successfully used for modelling NEE in this study. PAR was a significant control of daily NEE variations through its first-order control of photosynthesis. Model parameters for NEE for different microform types are presented in Table 5 in appendix. We observed different patterns in model performance when modelling NEE depending on if ETI or GAI was used for modelling. Models including ETI had a better performance for NEE at hummock and two of the *Carex* lawns; models including GAI performed better for NEE at all other microform types. Implementing an additional exponential term in the NEE model to reflect the dependency of R_{eco} on water table depth considerably improved the modelling results. Modelling of seasonal and daily variations in NEE fluxes was more successful at hollows as indicated by higher coefficients of determination than at hummocks (Table 2).

Regressions between R_{eco} and either water table or air temperature show that both environmental factors were important in explaining R_{eco} (Fig. 9). The corresponding modelled time series R_{eco} fluxes are shown in Fig. 7. We observed differences in the strength of the statistical relationship between air temperature and R_{eco} : hummocks were characterised by stronger relationships than lawns and hollows. The relationships between water table depth and R_{eco} were characterised by the same pattern. At all microforms, decreasing water table depth caused increasing respiration values. The effect of WT on R_{eco} had a sigmoid form at all hummock sites and ombrogenous lawns and at two *Carex* lawns; it was exponential at all hollow sites and minerogenous lawns and at one *Carex* lawn site where the range of water table depths was probably not sufficient for the fitting of a sigmoidal

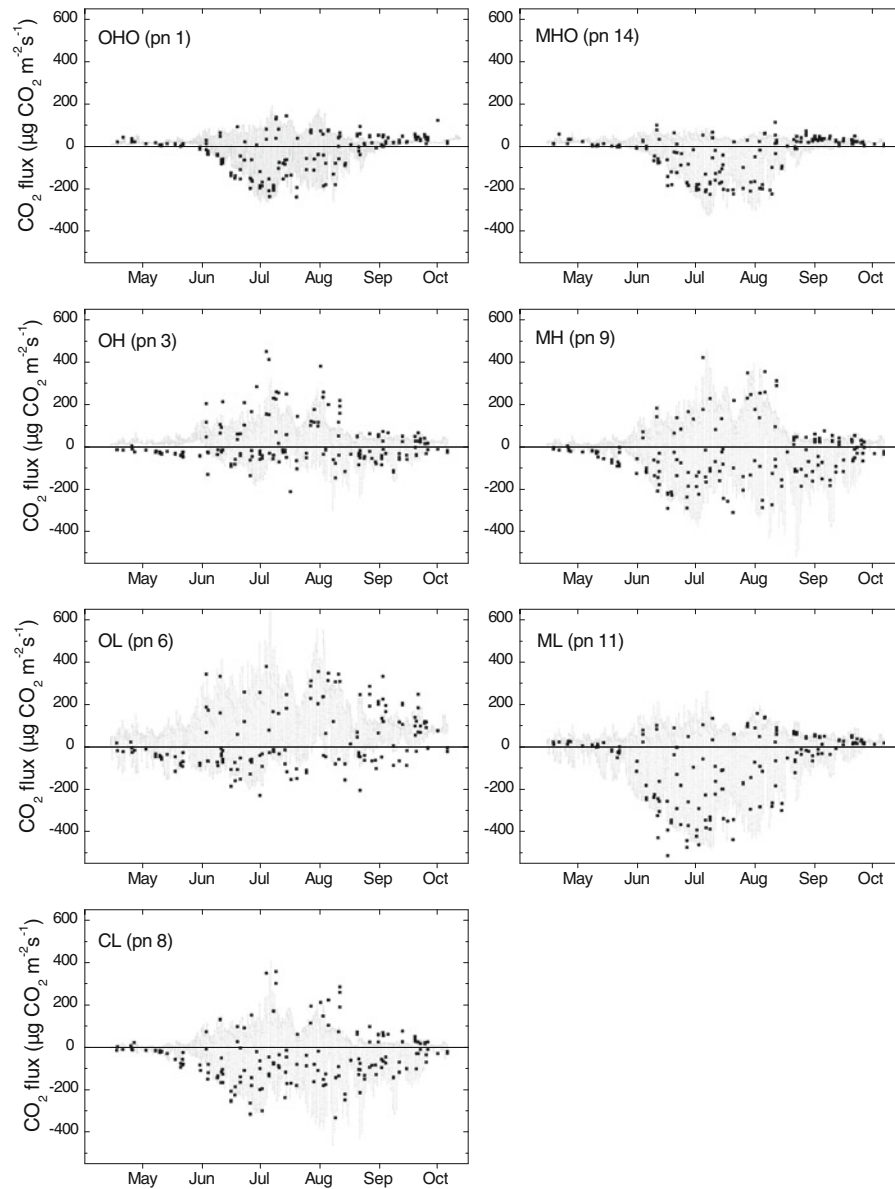


Fig. 6 Seasonal patterns of NEE at different microform types in Ust-Pojeg peatland over the investigated period; each microform type is represented by one plot. Microform acronyms are explained in Fig. 4 and the text. Please note that measured

NEE was determined for inside-chamber conditions (reduced PAR compared to ambient conditions) and therefore cannot be directly compared with modelled NEE which was calculated using ambient PAR as input variable

function (Fig. 9). The seasonal and daily variations in R_{eco} were best modelled for hummocks and lawns followed by hollows (Table 6 in appendix).

GPP was modelled based on PAR, air temperature and either GAI or ETI. Models based on ETI usually underestimated the GPP fluxes in spring, whereas models based on GAI usually underestimated the GPP fluxes in autumn, especially at hummock sites.

In terms of ETI and GAI, we observed a similar pattern as in modelling NEE fluxes: ETI had a better performance at hummocks and two of the *Carex* lawns, additionally at one ombrogenous hollow and minerogenous lawn. An implementation of the water table depth into GPP models did not improved the modelling results (results not shown). The GPP fluxes were best modelled for minerogenous lawns, followed

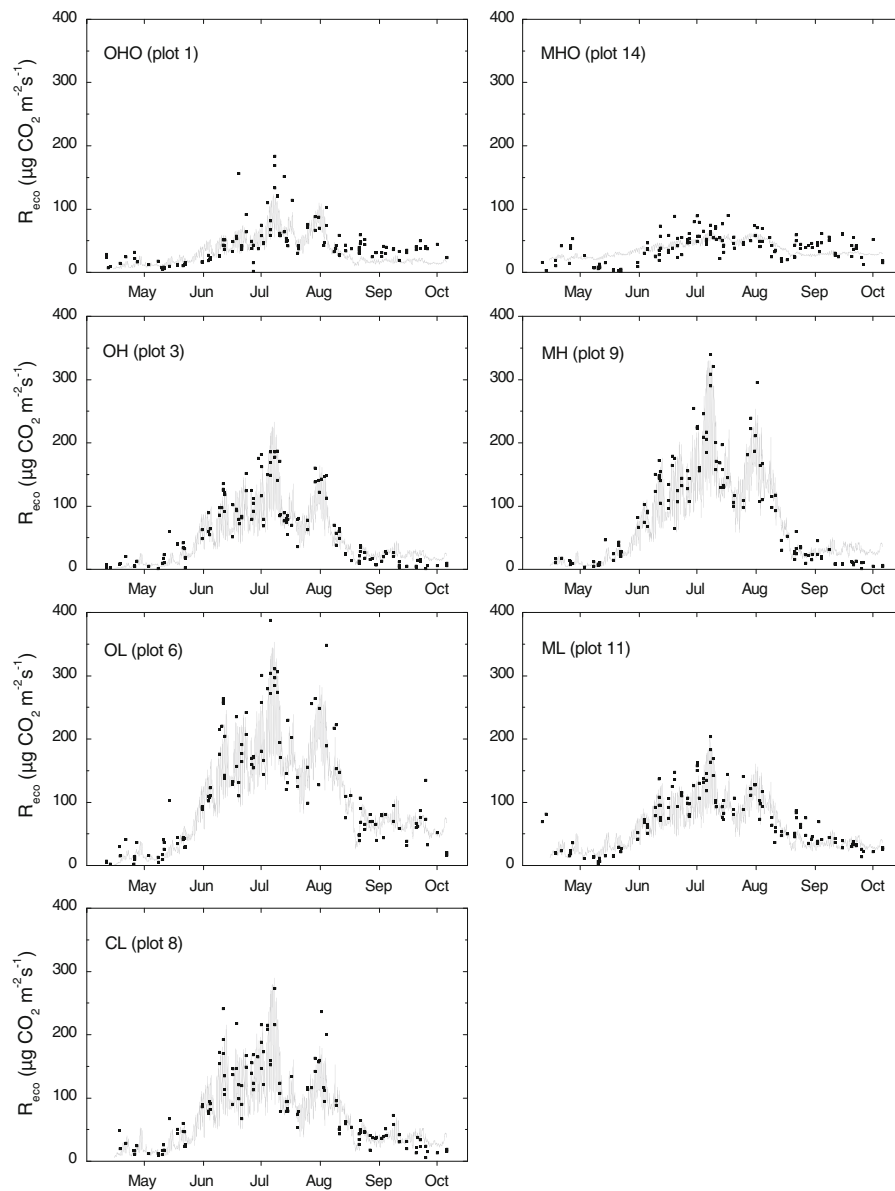


Fig. 7 CO_2 release due to ecosystem respiration (R_{eco}) at different microform types in Ust-Pojeg peatland over the investigation period; each microform type is represented by one plot as example. *Squares* indicate the seasonal patterns of

measured R_{eco} ; the *line* indicates the modelled R_{eco} fluxes within the chambers. Microform acronyms are explained in Fig. 4 and the text

by hollows, minerogenous hummocks and ombrogenous lawns (Table 7 in appendix).

The cumulative sums and errors of the modelled NEE over the season (Fig. 10) showed differences in seasonal NEE within and between various microform types of the Ust-Pojeg peatland. The difference in cumulative sums between the ombrogenous and minerogenous hollow sites was comparatively small: only

the CO_2 uptake during the summer was slightly higher at minerogenous hollow sites. The ombrogenous and minerogenous hummocks differed in the patterns of the modelled CO_2 exchange over the season. Compared to ombrogenous hummocks, the minerogenous hummocks showed lower values of cumulative NEE during the summer; one plot showed even negative values. Cumulative NEE at minerogenous lawns showed a

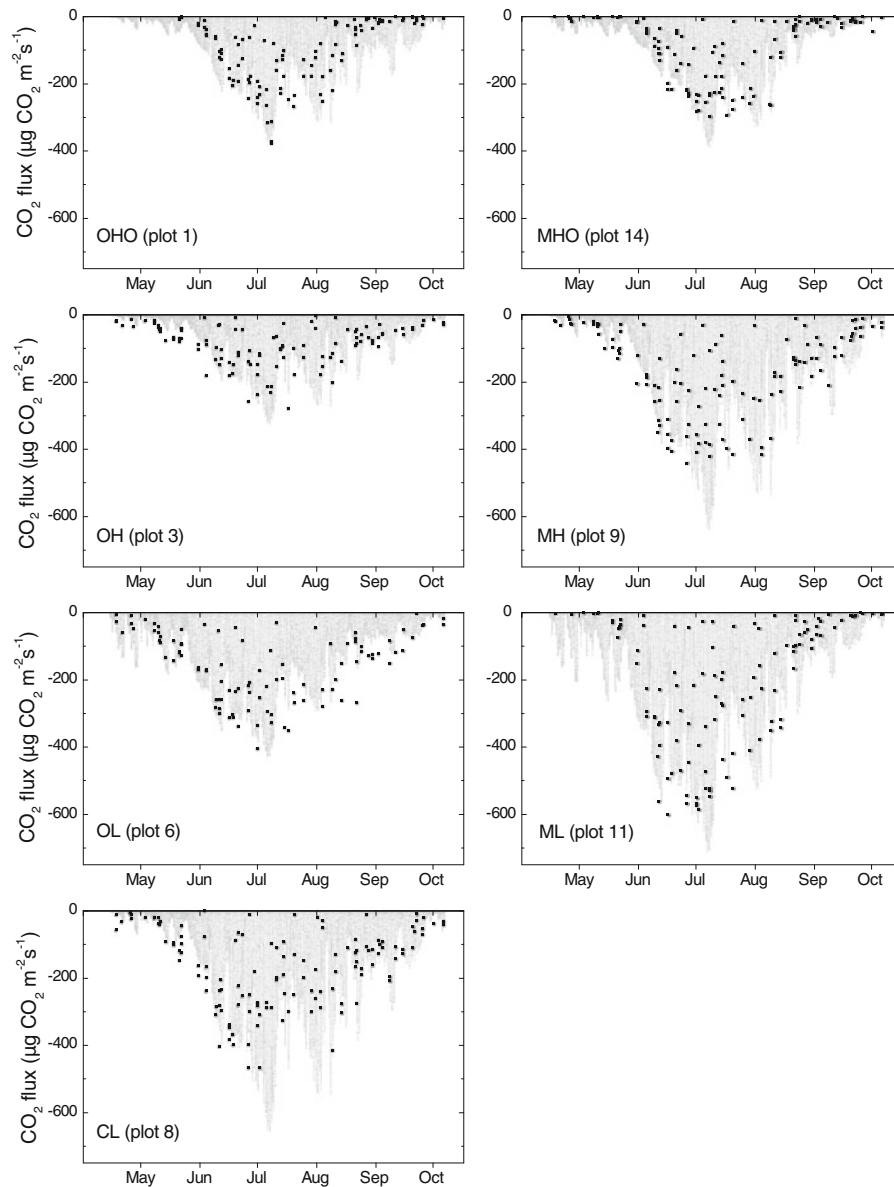


Fig. 8 Seasonal patterns of GPP at different microform types in Ust-Pojeg peatland over the investigated period; each microform type is represented by one plot as example. Microform acronyms are explained in Fig. 4 and the text. Measured GPP

step decline in summer meaning that the minerogenous lawns were strong CO_2 sinks during summer. The cumulative NEE of ombrogenous lawns was nearly continuously positive. The biggest differences between the replicates of one microform type were determined at minerogenous and ombrogenous lawns and *Carex* lawn sites.

was determined for inside-chamber conditions (reduced PAR compared to ambient conditions) and therefore cannot be directly compared with modelled GPP which was calculated using ambient PAR as input variable

Based on the modelled time series of NEE, the CO_2 budgets for all microform types were calculated (Fig. 10). During the period of observations, the CO_2 budget was estimated to be negative (CO_2 sink) for hollows, minerogenous lawns and one of the *Carex* lawns and minerogenous hummock sites, respectively, and positive (CO_2 source) for ombrogenous

hummocks and lawns and two *Carex* lawns and minerogenous hummocks, respectively.

It has been possible to model the NEE, R_{eco} and GPP fluxes with good agreements between modelled and measured CO_2 fluxes (Tables 5, 6, 7 in appendix; Fig. 11). The modelled data of NEE, R_{eco} and GPP showed that the regression models naturally give conservative predictions (Fig. 11); they underestimate high values and overestimate low values. The magnitude of over- and underestimation varies between the different microforms: modelling of CO_2 fluxes at flark sites is less affected compared to hummocks.

Comparison of two methods for NEE estimation

The comparison of the two different modelling methods to estimate the NEE fluxes showed that the method to model NEE directly ($\text{NEE}_{\text{mod-1}}$, using Eq. 2 or 3) was more successful (has higher Wilmott index of agreement) than the method to calculate NEE by summing up the modelled GPP and R_{eco} fluxes ($\text{NEE}_{\text{mod-2}}$) (Table 1). The difference between measured NEE (NEE_{meas}) and $\text{NEE}_{\text{mod-1}}$ and NEE_{meas} and $\text{NEE}_{\text{mod-2}}$ is less pronounced at hollow sites compared to hummock sites. The cumulative flux calculated over the investigation period showed a considerable difference between the two different methods of NEE estimation (Table 2). $\text{NEE}_{\text{mod-2}}$ results showed that the investigated plots were stronger CO_2 sinks or weaker CO_2 sources than modelled directly ($\text{NEE}_{\text{mod-1}}$).

Spatial upscaling

About 30% of the intensive study at the Ust-Pojeg peatland is covered by the minerogenous microforms, 17% by the *Carex* lawns and about 53% by ombrogenous microforms (MHO: 12%, ML: 9%, MH: 9%, CL: 17%, OHO: 18%, OL: 23%, OH: 12%). The land cover classification of the entire peatland showed that about 50% is covered by bogs and 50% by fens (Susiluoto, personal communication). The result of an area-weighted calculation of the NEE for the intensive study site was an average release of about $300 \pm 413 \text{ g CO}_2 \text{ m}^{-2}$ over the investigated period. The ombrogenous part was a strong CO_2 source ($281 \pm 180 \text{ g CO}_2 \text{ m}^{-2}$) while the minerogenous part was a weak CO_2 sink ($-22 \pm 142 \text{ g CO}_2 \text{ m}^{-2}$). If we would assume the lowest rate of CO_2 fluxes during the

Fig. 9 Relationships between water table depth and R_{eco} (left side) and between air temperature and R_{eco} (right side). Black dots indicate the measured CO_2 fluxes; the lines fitted sigmoidal and exponential curves according to Eqs. 4 and 5, respectively. Each microform type is represented by one plot as example. Microform acronyms are explained in Fig. 4 and the text

first measurement days in April to be representative for the winter fluxes and calculate the annual CO_2 budget based on this assumption, then the minerogenous part would change to a CO_2 source and the ombrogenous become an even stronger CO_2 source. The intensive study area would be an annual CO_2 source of about $700 \pm 600 \text{ g CO}_2 \text{ m}^{-2}$.

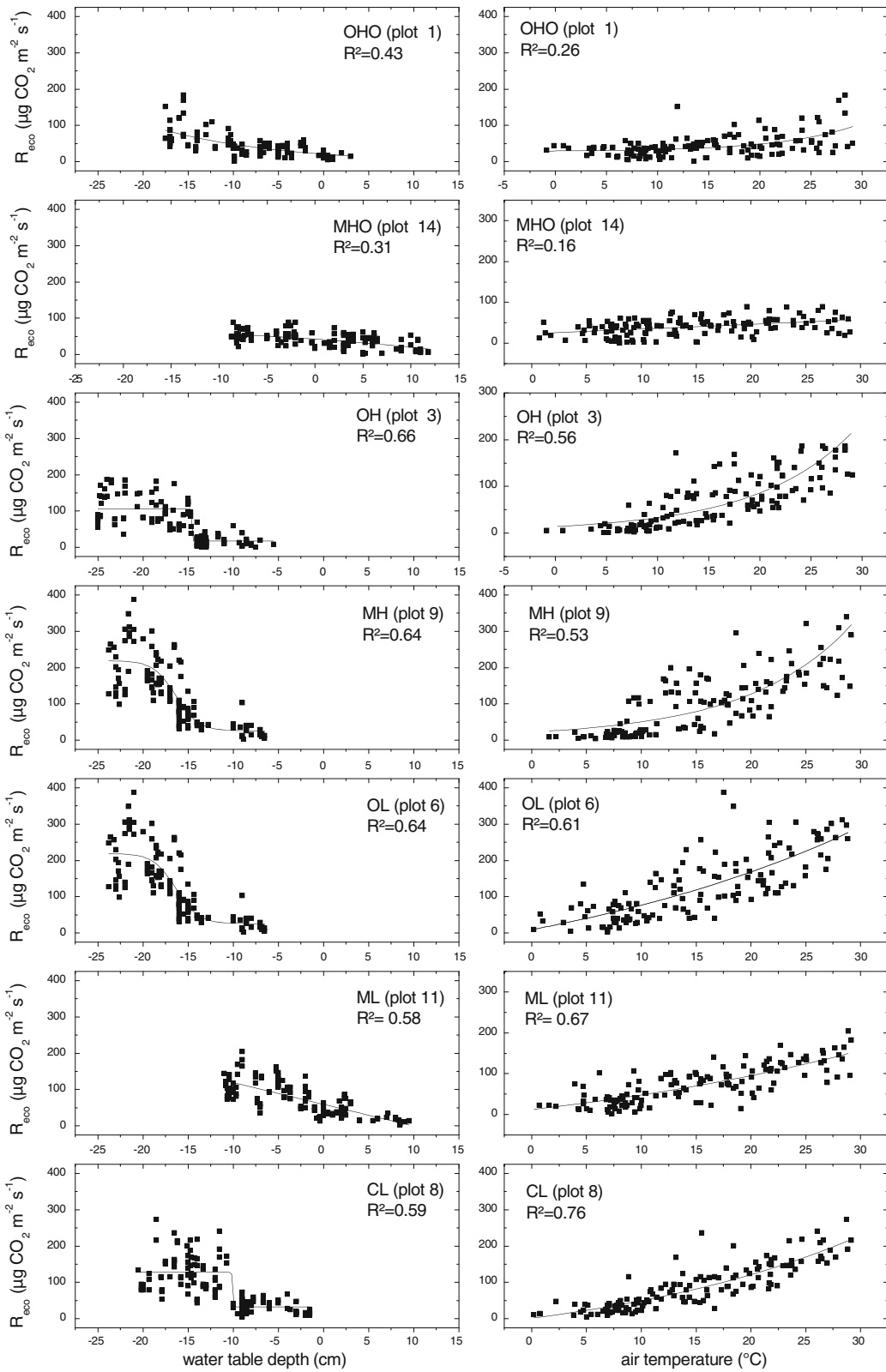
Discussion

Within-microform variability in CO_2 fluxes

We observed high spatial variability in measured NEE, R_{eco} and estimated GPP within microform types. *Carex* lawns and minerogenous lawns were the microform types with especially large variability of NEE within one microform type (Fig. 10). The reason for the differences within these *Carex* lawns probably derives from differences in the degree of vegetation cover of each plot's dominant species. The maximum GAI at plots which were densely covered with vegetation was 2.3 and 2.0 $\text{m}^2 \text{ m}^{-2}$ compared to 0.8 $\text{m}^2 \text{ m}^{-2}$ at less covered plot. This indicates that at plots with similar water table depths differences in GAI could have a strong effect on the strength of the CO_2 uptake.

Differences in NEE between the plots of the minerogenous lawns were probably caused by water table and vegetation characteristics. Compared to plot 13, plot 15 was characterised by a higher water level which we expected to lead to a stronger seasonal CO_2 net uptake; however, it unexpectedly showed a seasonal CO_2 net release. This difference is probably caused by the vegetation composition as its vegetation consisted partly of vegetation typically found at hummock sites. Thus, plot 15 showed the NEE pattern typical for hummocks despite the high water table level.

Also, differences in NEE fluxes between the plots of the ombrogenous hummocks could be observed. This difference could not be explained by differences in vegetation composition (mix of *Andromeda polifolia*, *Chamaedaphne calyculata*, *Oxycoccus palustris*



and *Sphagnum* spec.) and in GAI (1.8–2.5 m²m⁻²), as they were relatively similar. Probably, the difference in maximum water table depth of 11 cm between the two plots was related to the higher respiration rates of the plot with lower water table depth compared to the plot with higher water table depth. The lower water table depth implicated a greater aerated portion of the peat profile. This could have led to enhanced oxygen availability for microbial decomposition and root growth and thus to higher respiration rates (Bubier et al. 2003a).

Variability in CO₂ fluxes between microform types

The differences in CO₂ fluxes between microforms might be explained by differences in GAI and water table depth. Although minerogenous hollows were characterised by higher GAI than minerogenous lawns, they did not have a higher CO₂ uptake. Beside *Scheuchzeria palustris* and *Carex limosa*, *Utricularia intermedia* grew in minerogenous hollows. These submerged aquatic carnivorous plants are characterised by limited photosynthetic uptake of inorganic carbon (Adamec 1995), which might explain to some degree the lower CO₂ uptake in the minerogenous hollows compared to lawns. However, probably more important is the limitation of photosynthesis under submerged conditions. Minerogenous hollows were water-saturated during most of the investigation season, resulting in lower mean NEE, R_{eco} and GPP compared to minerogenous lawns. Mosses in peatlands are adapted to high water table levels, but very high water content in *Sphagnum* mosses slows down the CO₂ and O₂ exchange to the photosynthetically active tissues (Wallen et al. 1988), thus the environmental conditions at minerogenous lawns were more favourable for photosynthesis and respiration of mosses than at minerogenous hollows.

Water table depth influences photosynthesis as well as respiration. The lower GPP fluxes of the hummocks compared to lawns might be explained by the effect of surface dryness which occurred more often at hummocks and can lead to a reduction of photosynthesis of both vascular plants and *Sphagnum* mosses (Arneth et al. 2002). Water table depth and R_{eco} were related in the spatial domain: hummocks with the lowest water table showed the highest respiration while hollows with the highest water level showed the lowest respiration. Minerogenous lawns had intermediate

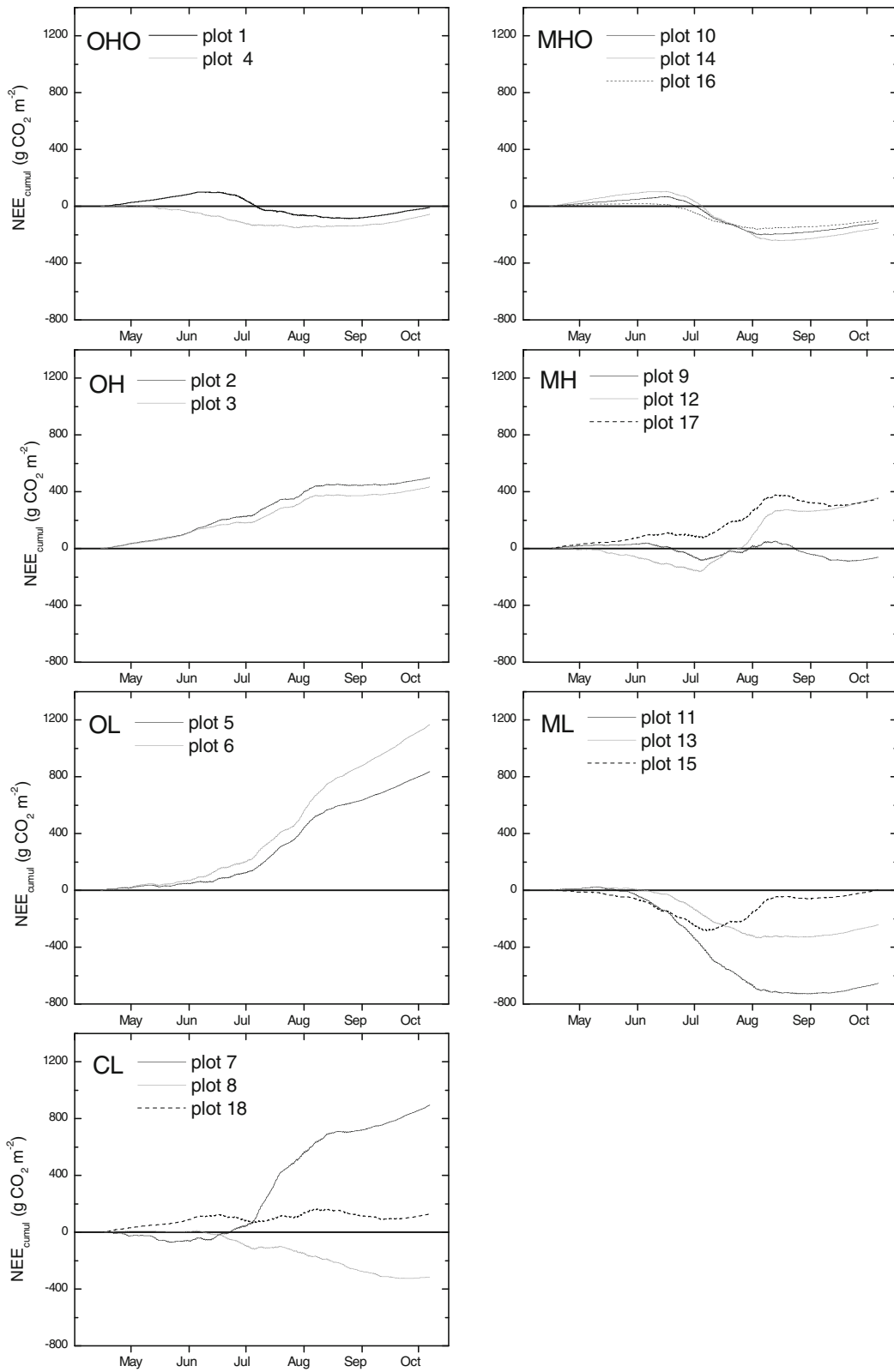
Fig. 10 Cumulative sums of modelled NEE ($NEE_{\text{mod-1}}$) fluxes under ambient PAR conditions for the investigation period 2008 for different microforms. Microform acronyms are explained in Fig. 4 and the text. Cumulative sums are also presented in Table 2

water levels and intermediate respiration. However, ombrogenous lawns were characterised by very high respiration fluxes. Lowering of the water table was found to cause an increase in ecosystem respiration (Oechel et al. 1993; Johnson et al. 1996). The main cause of increased ecosystem respiration is the increased peat decomposition and mineralisation under oxic conditions, which is probably the main component of R_{eco} (Silvola et al. 1996).

We contextualized our work by comparing it to similar studies (Table 3). Even though all study sites were located in the boreal zone, they are characterised by different climatic conditions, and the GAI of the microforms from different study sites may be different. While comparing the CO₂ fluxes measured at different study sites, we also have to be aware of the different weather condition during the investigation periods and different number of investigation periods. These differences in climate, weather and site conditions might explain the differences in CO₂ fluxes measured at different study sites. Studies by Riutta et al. (2007a) and Alm et al. (1997, 1999) at Finnish peatlands show the same range of CO₂ fluxes as measured at the Ust-Pojeg peatland even though the investigation period of the study by Alm et al. (1999) was characterised by a summer drought. The maximum R_{eco} fluxes at Ust-Pojeg are about double of the maximum R_{eco} fluxes measured by Riutta et al. (2007b), and the mean R_{eco} fluxes at Ust-Pojeg peatland are about four times the average R_{eco} estimated by Golovatskaya and Dyukarev (2009) but only half of the estimates by Griffis et al. (2000). We found contrary results to Waddington and Roulet (1996) who reported hummocks to be CO₂ sinks and hollows CO₂ sources.

Variability in CO₂ fluxes between ombrogenous and minerogenous parts of the peatland

At Ust-Pojeg peatland, differences in CO₂ fluxes between the minerogenous and ombrogenous parts of the study site were observed. Lindroth et al. (2007) described the coupling between peatland type and NEE as less obvious than between the long-term



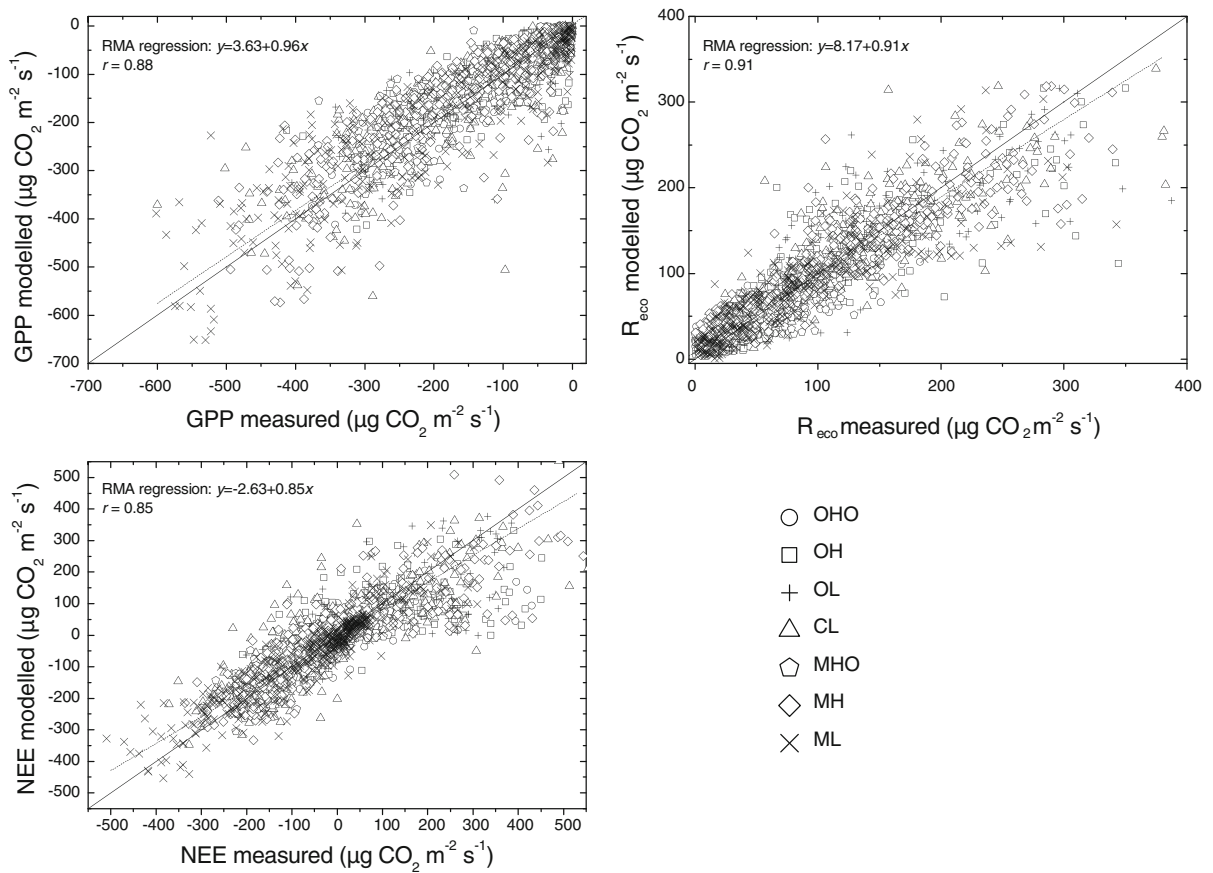


Fig. 11 Model performance for CO₂ net ecosystem exchange NEE (NEE_{mod-1}), ecosystem respiration *R*_{eco} and gross primary production GPP at different microforms. The 1:1 line indicating

a perfect match and reduced major axis (RMA) regression lines are shown. Microform acronyms are explained in Fig. 4 and the text

Table 1 Willmott index of agreement (*d*_W) of two different modelling methods for estimation of NEE: (1) by applying the empirical models derived from fitting Eq. 2 or 3 directly to the NEE measurement data (NEE_{mod-1}) and (2) by calculating the NEE time series from the sums of the modelled values of *R*_{eco}

and GPP derived from fitting Eqs. 4 and 5 to the *R*_{eco} measurements and Eqs. 6 and 7 to the GPP estimates, respectively (NEE_{mod-2}). *d*_W = 1 indicates a perfect match to the measured data

	Plot number	<i>d</i> _W (NEE _{mod-1})	<i>d</i> _W (NEE _{mod-2})	Plot number	<i>d</i> _W (NEE _{mod-1})	<i>d</i> _W (NEE _{mod-2})	Plot number	<i>d</i> _W (NEE _{mod-1})	<i>d</i> _W (NEE _{mod-2})
OHO	1	0.91	0.84	OH	2	0.75	OL	5	0.83
	4	0.90	0.81		3	0.84		6	0.87
MHO	10	0.94	0.89	MH	9	0.95	ML	11	0.97
	14	0.97	0.94		12	0.90		13	0.96
	16	0.94	0.92		17	0.92		15	0.93
							CL	7	0.85
								8	0.93
								18	0.93

Table 2 Cumulative flux calculated using two different modelling methods for estimation of NEE: (1) by applying the empirical models derived from fitting Eq. 2 or 3 directly to the NEE measurement data ($NEE_{\text{cumul-mod-1}}$) and (2) by calculatingthe NEE time series from the sums of the modelled values of R_{eco} and GPP derived from fitting Eqs. 4 and 5 to the R_{eco} measurements and Eqs. 6 and 7 to the GPP estimates, respectively ($NEE_{\text{cumul-mod-2}}$)

Plot number	$(NEE_{\text{cumul-mod-1}})$ (g m^{-2})	$(NEE_{\text{cumul-mod-2}})$ (g m^{-2})	Plot number	$(NEE_{\text{cumul-mod-1}})$ (g m^{-2})	$(NEE_{\text{cumul-mod-2}})$ (g m^{-2})	Plot number	$(NEE_{\text{cumul-mod-1}})$ (g m^{-2})	$(NEE_{\text{cumul-mod-2}})$ (g m^{-2})			
OHO	1	-8 ± 8	-236 \pm 10	OH	2	499 \pm 18	448 \pm 16	OL	5	837 \pm 14	267 \pm 15
	4	-56 ± 9	-330 \pm 11		3	435 \pm 11	112 \pm 13		6	1,169 \pm 14	398 \pm 17
MHO	10	-115 ± 6	-86 \pm 8	MH	9	-61 ± 9	-184 \pm 13	ML	11	-654 ± 9	-774 ± 11
	14	-154 ± 5	-199 \pm 6		12	359 \pm 14	34 \pm 18		13	-242 ± 8	-416 ± 9
	16	-98 ± 5	-141 \pm 5		17	352 \pm 6	-151 \pm 32		15	4 \pm 11	-124 ± 13
								CL	7	896 \pm 23	224 \pm 25
									8	-315 ± 9	-211 ± 12
									18	128 \pm 11	-278 ± 12

average peat carbon accumulation rate and peatland type. However, Bubier et al. (1999) reported an increase in photosynthesis and respiration from bogs over poor fen, intermediate fen to rich fen. At the investigated peatland, this result was only found for some microform types, for example for R_{eco} and GPP fluxes at hummock sites and for GPP only at lawns. The results of our study confirm the findings of Bubier et al. (1999) that a poor fen is a stronger CO_2 sink than a bog. In the case of the Ust-Pojeg peatland, the ombrogenous part of the peatland is even a CO_2 source. The minerogenous and ombrogenous part of the Ust-Pojeg peatland do not only differ in pH (5 and 4 for minerogenous and ombrogenous part, respectively) and C/N values (42 and 65 for minerogenous and ombrogenous part, respectively) (Wolf 2009) but also in water table depth, thus one of the reasons for the different CO_2 fluxes of ombrogenous and minerogenous hummocks in summer could be that the distance to the water table is greater at the ombrogenous hummocks. Thus, the impact of relatively dry conditions in July could have been stronger at the ombrogenous hummocks.

Seasonal cycle of CO_2 fluxes

The timing of the snow melt and the hydrometeorological conditions during the growing season control the CO_2 exchange of boreal peatlands (Aurela et al. 2004). At the Ust-Pojeg study site, April and May were colder than the ten-year average. Warmer

weather occurred in the second half of June, this is about two weeks later than on average. Studies by Friborg et al. (1997), Aurela et al. (2004) and Moore et al. (2006) showed that the spring period controls the annual CO_2 balance of peatlands. The snow melt timing is important as it determines the onset of the photosynthesis which is associated with moss activity followed by the activity of the evergreen shrubs. Compared to other years, the spring 2008 was colder, and the snow melt started later. The low air and soil temperatures, the snowmelt water and the slow vegetation development limited the photosynthetic activity in spring 2008. Hummocks are the microforms which are the most elevated compared to other microform types which leads to a faster snow melt, warming of the soil and vegetation development and thus to earlier CO_2 uptake. This early onset of photosynthesis at the hummocks was likely associated with the mosses which can photosynthesize as soon as the snow disappears and they receive light (Moore et al. 2006), and hummocks were snow-free earlier than other microform types. The mean air temperature of the summer months June, July and August agreed well with the ten-year average temperature. However, CO_2 exchange is sensitive to variations in environmental factors on the short-term scale, for example, GPP and R_{eco} decreased due to a strong decrease in air temperature at the end of July and beginning of August. In October, the air temperatures were higher than the ten-year average which probably led to enhanced respiration but not to increased photosynthesis because the

Table 3 Review of CO₂ fluxes measured by closed chamber technique at pristine boreal peatlands

Location	Reference	Characteristics	Comparison parameter	Other study	This study	
Finland 62°47'N 30°56'E	Alm et al. (1997)	Low sedge-sphagnum-pine fen	Hummock	GPP	-1151.5 g CO ₂ m ⁻² ip ⁻¹	-1243 ± 115 g CO ₂ m ⁻² ip ^{-1a}
				R _{eco}	755.5 g CO ₂ m ⁻² ip ⁻¹	1255 ± 141 g CO ₂ m ⁻² ip ^{-1a}
		Carex lawn	Hummock	GPP	-1162.5 g CO ₂ m ⁻² ip ⁻¹	-1233 ± 115 g CO ₂ m ⁻² ip ^{-1a}
				R _{eco}	601.5 g CO ₂ m ⁻² ip ⁻¹	1192 ± 390 g CO ₂ m ⁻² ip ^{-1a}
		Hollow	Hummock	GPP	-825 g CO ₂ m ⁻² ip ⁻¹	-692 ± 62 g CO ₂ m ⁻² ip ^{-1a}
				R _{eco}	403.5 g CO ₂ m ⁻² ip ⁻¹	516 ± 43 g CO ₂ m ⁻² ip ^{-1a}
Finland 62°50'N 30°53'E	Alm et al. (1999)	Open sphagnum bog	Hummock	GPP	-627 g CO ₂ m ⁻² ip ⁻¹	-816 ± 230 g CO ₂ m ⁻² ip ^{-1a}
				R _{eco}	1056 g CO ₂ m ⁻² ip ⁻¹	1051 ± 423 g CO ₂ m ⁻² ip ^{-1a}
		Sphagnum angustifolium lawn	Hummock	GPP	-861 g CO ₂ m ⁻² ip ⁻¹	-989 ± 141 g CO ₂ m ⁻² ip ^{-1a}
				R _{eco}	711 g CO ₂ m ⁻² ip ⁻¹	1361 ± 202 g CO ₂ m ⁻² ip ^{-1a}
		Hollow	Hummock	GPP	-689 g CO ₂ m ⁻² ip ⁻¹	-820 ± 66 g CO ₂ m ⁻² ip ^{-1a}
				R _{eco}	726 g CO ₂ m ⁻² ip ⁻¹	524 ± 32 g CO ₂ m ⁻² ip ^{-1a}
Canada 58°N45'N 94°04'W	Griffis et al. (2000)	Fen	Small hummock	Mean GPP ^b	-8.8 g CO ₂ m ⁻² d ⁻¹	-5.9 g CO ₂ m ⁻² d ⁻¹
				Mean R _{eco} ^b	9.9 g CO ₂ m ⁻² d ⁻¹	5.4 g CO ₂ m ⁻² d ⁻¹
		Large hummock	Small hummock	Mean GPP ^b	-5.1 g CO ₂ m ⁻² d ⁻¹	
				Mean R _{eco} ^b	5.5 g CO ₂ m ⁻² d ⁻¹	
		Hollow	Small hummock	Mean GPP ^b	-2.1 g CO ₂ m ⁻² d ⁻¹	-3.4 g CO ₂ m ⁻² d ⁻¹
				Mean R _{eco} ^b	3.4 g CO ₂ m ⁻² d ⁻¹	1.8 g CO ₂ m ⁻² d ⁻¹
Russia 56°58'N 82°36'E	Golovatskaya and Dyukarev (2009)	Low pine-shrub-sphagnum bog sedge-sphagnum fen	Mean R _{eco} of snow free season	105.6 ± 27.2 mg CO ₂ m ⁻² h ^{-1c}	448 ± 561 mg CO ₂ m ⁻² h ^{-1d}	
				112.4 ± 39.4 mg CO ₂ m ⁻² h ^{-1c}	317 ± 386 mg CO ₂ m ⁻² h ^{-1d}	
Finland 61°47'N 24°18'E	Riutta et al. (2007b)	Oligotrophic fen	Maximum GPP	-1,316 mg CO ₂ m ⁻² h ⁻¹	-1,337 mg CO ₂ m ⁻² h ⁻¹	
				Maximum R _{eco}	561 mg CO ₂ m ⁻² h ⁻¹	1,235 mg CO ₂ m ⁻² h ⁻¹
Sweden 63°44'N 20°06'E	Waddington and Roulet (1996)	Eccentric raised bog	Hummock	NEE	180 g CO ₂ m ⁻² , -58.7 g CO ₂ m ⁻² ip ⁻¹	627.6 ± 12.4 g CO ₂ m ⁻² ip ⁻¹
				Hollow		96 g CO ₂ m ⁻² , 1288 g CO ₂ m ⁻² ip ⁻¹
				IP: May–September	IP: May–September	

Table 3 continued

Location	Reference	Characteristics	Comparison parameter	Other study	This study
Finland 61°47'N 24°18'E	Riutta et al. (2007a)	Oligotrophic fen	Mean GPP	−1170 g CO ₂ m ^{−2} ip ^{−1e}	−1040 g CO ₂ m ^{−2} ip ^{−1f}
			Mean <i>R</i> _{eco}	810 g CO ₂ m ^{−2} ip ^{−1e}	856 g CO ₂ m ^{−2} ip ^{−1f}
			Mean NEE	−430 g CO ₂ m ^{−2} ip ^{−1e}	−50 g CO ₂ m ^{−2} ip ^{−1f}
				IP: May–October	IP: May–October

IP investigation period

^a Mean of respective measurement plots and standard deviation

^b June–August

^c Mean of 8 investigation periods

^d Mean of measured values at ombrogenous and minerogenous part, respectively

^e Mean of 4 investigation periods

^f Mean of all measurement plots in minerogenous part weighted by area

senescence of the vegetation plays an important role for the photosynthetic activity. Photosynthesis at hummocks was strong in the beginning and at the end of the growing season probably due to the shrubs and mosses as explained above. The increasing air temperature and water table drawdown over the season controlled the seasonal cycle of *R*_{eco} leading to maximum values around 22nd July. The reason for the timing of the maximum values of the GPP laid in the phenological development of the vegetation period.

Balance of CO₂ exchange between the atmosphere and the peatland

Studies by Alm et al. (1997), Riutta et al. (2007a) and Sagerfors et al. (2008) reported that boreal fens and ombrotrophic bogs (Moore et al. 2002) were CO₂ sinks. Our study site is characterised by minerogenous and ombrogenous parts; the minerogenous part was a weak CO₂ sink and the ombrogenous part a clear CO₂ source. One explanation for the differing results from the ombrogenous part of the Ust-Pojeg peatland could be that the investigation period of this study was longer than some of the previous closed chamber studies in northern peatlands (Waddington and Roulet 1996; Alm et al. 1997; Bubier et al. 2003b) including also spring and autumn which were characterised by CO₂ release rather than by CO₂ uptake. This could be one of the reasons for some of the microforms being a CO₂ source over the investigated period. Shurpali et al. (1995) showed in their study that a boreal

ecosystem can be a CO₂ source on a dry year but a sink in the following wet year, highlighting the importance of long-term studies. Did hot and warm summer conditions also influence the CO₂ fluxes at Ust-Pojeg peatland? As described above, the air temperature during the summer of the investigation period was similar to average values, and the precipitation was above average values, so the vegetation did not experience extreme drought during that year. Thus, it is rather unlikely that summer drought could be the reason for the ombrogenous part being a CO₂ source during the investigation period in 2008. Despite the interannual variations in temperature and precipitation, further external drivers may include long-term changes in mineral nutrient supply generated by anthropogenic activity. For example, improved nitrogen supply could lead to increased peat decomposition and loss of carbon (Franzén 2006). In the case of the Ust-Pojeg peatland the source of anthropogenic emissions could be the nearby city of Syktyvkar.

Measurements by the closed chamber technique are often used for CO₂ flux estimations, not only on the microform scale but also on ecosystem and regional scales. Our study shows that it is not only important to calculate the area covered by the different microform types but also to consider the differences in CO₂ fluxes within a microform type. At our study site, the differences in GAI were especially important, which possibly could be obtained by remote sensing techniques. This method of area estimates would probably be more precise, and thus the uncertainty of the

upscaled fluxes would be less. Including high-resolution spatial vegetation information could also improve the agreement between CO₂ fluxes measured by different techniques in the same ecosystem but on different scales, as for example the closed chamber technique and the eddy covariance approach.

Summary and conclusions

As a contribution to the still rather sparse data on atmospheric CO₂ fluxes from boreal peatlands in Russia, this paper presents data on the net ecosystem exchange of CO₂ as well as CO₂ release by ecosystem respiration and CO₂ uptake by gross primary production which were recorded using the closed chamber method at a boreal peatland ecosystem in the Komi Republic, Russia. This study stands out also due to the long measurement period over the complete growing season and the high temporal frequency of measurements. We studied the influence of different environmental factors on the CO₂ fluxes at the microform scale. Such data are extremely scarce for the extensive peatlands in Russia. Water table and green area index (GAI) were found to have strong influence on CO₂ fluxes both between different microforms as well as within different patches of the same microform type. In the Ust-Pojeg peatland, strong differences in CO₂ fluxes within one microform type could be observed; for example, *Carex* lawns with low maximum GAI

were CO₂ sources over the investigation period, but *Carex* lawns with high maximum GAI values were CO₂ sinks. Although the minerogenous and ombrogenous parts of the Ust-Pojeg peatland were located close to each other, the differences in CO₂ fluxes were strong; over the investigation period the minerogenous part was a weak CO₂ sink, and the ombrogenous part was a pronounced CO₂ source. However, both were estimated to be CO₂ sources on an annual time scale.

Acknowledgments We gratefully acknowledge the contribution of M. Gažovič, J. Ibendorf, O. Michajlov, M. Miglovec, P. Schreiber, C. Wille and U. Wolf for assisting us in carrying out the CO₂ flux chamber measurements and of S. Susiluoto (University of Helsinki) and I. Beil for producing the maps. We thank N. Goncharova and J. Severin for their help in carrying out the vegetation survey and B. Runkle for revising the language and for his comments which improved the manuscript. The main funding for the project was provided by the EU Project “CarboNorth” (036993), the German Science Foundation (WI-2680 1/1 and 2/1) and a Sofja Kovalevskaja Research Award to M. Wilking. During the period of data analysis and manuscript preparation, L. Kutzbach was supported through the Cluster of Excellence “CliSAP” (EXC177), University of Hamburg, funded through the German Science Foundation (DFG).

Appendix

Description of measurement plots, model parameters, coefficient of determination, root mean square error, *F* values and levels of significance.

Table 4 Predominant vegetation (with coverage, %), microform type, mean water table depth (with range in parenthesis, the minus sign was used when the water table was above the

surface) for the investigation period and maximum GAI of all measurement plots in the Ust-Pojeg peatland, 2008

Plot number	Microform type	Vegetation	Cover (%)	Water table (cm)	Maximum GAI (m ² m ⁻²)
1	OHO	<i>Scheuchzeria palustris</i>	10	6 (–5 to 18)	1.2
		<i>Oxycoccus palustris</i>	5		
		<i>Sphagnum angustifolium</i>	90		
2	OH	<i>Chamaedaphne calyculata</i>	10	26 (17–37)	0.28
		<i>Oxycoccus palustris</i>	5		
		<i>Sphagnum magellanicum</i>	65		
		<i>Sphagnum angustifolium</i>	30		
		<i>Polytrichum strictum</i>	5		

Table 4 continued

Plot number	Microform type	Vegetation	Cover (%)	Water table (cm)	Maximum GAI (m ² m ⁻²)
3	OH	<i>Chamaedaphne calyculata</i>	15	15 (4–25)	0.18
		<i>Sphagnum magellanicum</i>	90		
		<i>Sphagnum angustifolium</i>	10		
4	OHO	<i>Scheuchzeria palustris</i>	10	9 (–3 to 19)	0.42
		<i>Oxycoccus palustris</i>	5		
		<i>Sphagnum angustifolium</i>	100		
5	OL	<i>Scheuchzeria palustris</i>	10	12 (2–21)	0.54
		<i>Carex limosa</i>	10		
		<i>Oxycoccus palustris</i>	15		
		<i>Sphagnum angustifolium</i>	100		
6	OL	<i>Andromeda polifolia</i>	10	16 (1–24)	0.61
		<i>Oxycoccus palustris</i>	10		
		<i>Chamaedaphne calyculata</i>	5		
		<i>Sphagnum angustifolium</i>	100		
7	CL	<i>Carex rostrata</i>	15	10 (1–21)	0.76
		<i>Carex limosa</i>	10		
		<i>Oxycoccus palustris</i>	15		
		<i>Sphagnum angustifolium</i>	80		
		<i>Sphagnum magellanicum</i>	20		
8	CL	<i>Carex rostrata</i>	50	10 (1–21)	2.33
		<i>Oxycoccus palustris</i>	15		
		<i>Sphagnum angustifolium</i>	90		
9	MH	<i>Andromeda polifolia</i>	15	11 (1–21)	1.39
		<i>Sphagnum magellanicum</i>	80		
		<i>Sphagnum angustifolium</i>	20		
10	MHO	<i>Scheuchzeria palustris</i>	45	1 (–10 to 11)	2.54
		<i>Utricularia intermedia</i>	80		
		<i>Sphagnum jensenii</i>	45		
11	ML	<i>Scheuchzeria palustris</i>	50	1 (–10 to 11)	1.32
		<i>Utricularia intermedia</i>	25		
		<i>Sphagnum subsecundum</i>	45		
		<i>Sphagnum jensenii</i>	40		
12	MH	<i>Sphagnum angustifolium</i>	5	11 (1–21)	1.73
		<i>Andromeda polifolia</i>	25		
		<i>Drosera rotundifolia</i>	10		
		<i>Sphagnum magellanicum</i>	80		
		<i>Sphagnum angustifolium</i>	15		
13	ML	<i>Polytrichum strictum</i>	5	8 (–3 to 18)	1.47
		<i>Andromeda polifolia</i>	15		
		<i>Oxycoccus palustris</i>	25		
		<i>Scheuchzeria palustris</i>	25		
		<i>Sphagnum angustifolium</i>	85		
14	MHO	<i>Sphagnum jensenii</i>	10	–2 (–12 to 9)	3.59
		<i>Scheuchzeria palustris</i>	25		
		<i>Sphagnum jensenii</i>	75		

Table 4 continued

Plot number	Microform type	Vegetation	Cover (%)	Water table (cm)	Maximum GAI (m ² m ⁻²)
15	ML	<i>Andromeda polifolia</i>	25	5 (–5 to 16)	2.30
		<i>Scheuchzeria palustris</i>	50		
		<i>Sphagnum subsecundum</i>	55		
		<i>Sphagnum jensenii</i>	45		
16	MHO	<i>Scheuchzeria palustris</i>	15	–2 (–8 to 6)	2.65
		<i>Carex limosa</i>	20		
		<i>Menyanthes trifoliata</i>	20		
		<i>Utricularia intermedia</i>	80		
17	MH	<i>Sphagnum jensenii</i>	15	7 (–1 to 14)	2.30
		<i>Betula nana</i>	30		
		<i>Andromeda polifolia</i>	10		
		<i>Oxycoccus palustris</i>	10		
18	CL	<i>Sphagnum magellanicum</i>	80	9 (2–17)	2.00
		<i>Sphagnum angustifolium</i>	20		
		<i>Carex rostrata</i>	40		
		<i>Oxycoccus palustris</i>	10		
		<i>Sphagnum angustifolium</i>	80		
		<i>Sphagnum magellanicum</i>	20		

Microform acronyms: ombrogenous hollows (OHO), lawns (OL) and hummocks (OH), and minerogenous hollows (MHO), lawns (ML) and hummocks (MH), and *Carex rostrata* lawns (CL)

Table 5 NEE model (Eqs. 2 and 3) parameter values (P_1 if modelled based on GAI in $\mu\text{g CO}_2 \text{ m}^{-2} \text{ s}^{-1} \text{ } ^\circ\text{C}^{-1}$, if modelled based on ETI in $\mu\text{g CO}_2 \text{ m}^{-2} \text{ s}^{-1} \text{ } ^\circ\text{C}^{-2}$; k_1 in $\mu\text{mol CO}_2 \text{ m}^{-2} \text{ s}^{-1}$; a_1 in $\mu\text{g CO}_2 \text{ m}^{-2} \text{ s}^{-1}$; b_1 in $^\circ\text{C}^{-1}$; c_1 in cm^{-1}) and their standard errors in parentheses, coefficient of determination (R^2), root mean square error (RMSE in $\mu\text{g CO}_2 \text{ m}^{-2} \text{ s}^{-1}$), F value and number of measurements (N) for all plots

Microform type	Plot number	GAI/ETI	P_1	k_1	a_1	b_1	c_1	R^2	F value	RMSE	N
OHO	1	GAI ^a	–17.0*** (2.1)	140.0** (66.6)	14.3*** (5.7)	0.06*** (0.01)	–0.07*** (0.02)	0.72***	106.3	51.6	168
		ETI	–2.9*** (0.6)	255.2* (142.5)	33.8*** (12.5)	0.05*** (0.02)	–0.007 ^{NS} (0.02)	0.65***	74.6	58.3	168
	4	GAI ^a	–19.7*** (2.3)	125.3*** (50.1)	26.4*** (9.0)	0.08*** (0.01)	–0.03** (0.01)	0.70***	91.5	57.9	164
		ETI	–3.8*** (2.7)	296.4* (142.1)	7.4** (4.8)	0.08*** (0.02)	–0.09*** (0.03)	0.65***	73.6	62.3	164
OH	2	GAI	–27.4*** (8.3)	365.7 ^{NS} (352.2)	6.1 ^{NS} (11.2)	0.1*** (0.02)	–0.04 ^{NS} (0.04)	0.30***	12.0	121.0	120
		ETI ^a	–5.3*** (2.1)	571.1 ^{NS} (523.5)	4.9 ^{NS} (4.9)	0.08*** (0.02)	–0.07*** (0.03)	0.42***	20.4	110.3	120
	3	GAI	–20.1*** (3.1)	150.3* (85.9)	25.1** (10.4)	0.08*** (0.01)	–0.04*** (0.01)	0.57***	53.4	70.2	168
		ETI ^a	–3.6*** (0.8)	345.9* (201.1)	10.0** (5.1)	0.07*** (0.01)	–0.08*** (0.02)	0.57***	53.0	70.3	168

Table 5 continued

Microform type	Plot number	GAI/ ETI	P_1	k_1	a_1	b_1	c_1	R^2	F value	RMSE	N
OL	5	GAI ^a	−19.1*** (3.7)	180.3* (120.2)	31.8** (13.6)	0.05*** (0.01)	−0.07*** (0.02)	0.55***	44.3	88.8	153
		ETI	−4.3** (1.9)	601.3 ^{NS} (604.3)	11.7 ^{NS} (8.7)	0.04* (0.02)	−0.1*** (0.04)	0.41***	26.1	100.9	153
	6	GAI ^a	−25.6*** (3.4)	113.8** (53.4)	34.2*** (11.5)	0.07*** (0.01)	−0.06*** (0.01)	0.62***	60.6	87.8	152
		ETI	−5.5*** (1.4)	401.1* (260.5)	11.2* (6.7)	0.06*** (0.01)	−0.01*** (0.03)	0.48***	33.9	103.1	152
CL	7	GAI ^a	−33.9*** (8.0)	380.2 ^{NS} (275.0)	21.5* (13.2)	0.07*** (0.01)	−0.11*** (0.03)	0.57***	40.1	142.7	126
		ETI	−9.6** (4.0)	818.0 ^{NS} (721.8)	12.0 ^{NS} (9.0)	0.07*** (0.02)	−0.14*** (0.03)	0.55***	36.3	146.7	126
	8	GAI	−31.0 ^{NS} (34.5)	2227.8 ^{NS} (3270.6)	0.14 ^{NS} (0.38)	0.12** (0.05)	−0.22** (0.11)	0.49***	37.8	88.0	165
		ETI ^a	−5.1*** (0.6)	278.0*** (90.6)	5.0** (2.6)	0.1*** (0.01)	−0.11*** (0.02)	0.77***	136.5	58.4	165
	18	GAI	−12.8*** (1.7)	166.3** (76.5)	12.3** (6.1)	0.1*** (0.01) (0.02)	−0.09*** (0.02)	0.69***	68.6	77.9	130
		ETI ^a	−5.6*** (0.7)	257.4*** (84.7)	18.2*** (7.0)	0.08*** (0.01)	−0.09*** (0.02)	0.78***	109.7	65.5	130
MHO	10	GAI ^a	−6.4*** (0.6)	121.9*** (46.2)	18.2*** (5.4)	0.09*** (0.01)	−0.02 ^{NS} (0.02)	0.81***	170.4	38.9	164
		ETI	−2.8*** (0.5)	293.6* (153.2)	22.0** (9.4)	0.07*** (0.02)	0.03 ^{NS} (0.03)	0.71***	97.2	48.2	164
	14	GAI ^a	−4.6*** (0.5)	160.6*** (57.0)	20.7*** (6.7)	0.07*** (0.01)	0.01 ^{NS} (0.02)	0.87***	275.2	31.7	164
		ETI	−2.1*** (0.3)	149.9** (74.6)	23.5** (11.6)	0.05** (0.02)	0.06 ^{NS} (0.04)	0.75***	121.7	44.2	164
16	GAI ^a	−5.0*** (0.5)	135.0*** (53.2)	17.9*** (6.5)	0.08*** (0.01)	−0.04** (0.02)	0.81***	137.3	31.4	132	
	ETI	−1.8*** (0.5)	437.5 ^{NS} (312.8)	8.8 ^{NS} (9.1)	0.04 ^{NS} (0.04)	0.2* (0.1)	0.71***	78.3	38.9	132	
MH	9	GAI	−19.2*** (1.7)	143.2*** (43.6)	13.1*** (4.3)	0.09*** (0.01)	−0.09*** (0.01)	0.78***	140.0	64.4	167
		ETI ^a	−6.7*** (0.6)	242.0*** (60.1)	9.4*** (3.1)	0.09*** (0.01)	−0.11*** (0.01)	0.83***	191.3	56.9	167
	12	GAI ^a	−14.1*** (1.8)	179.8** (76.3)	14.6** (6.6)	0.08*** (0.01)	−0.09*** (0.02)	0.70***	90.8	84.6	160
		ETI	−6.1*** (1.0)	360.1** (155.7)	5.9* (3.5)	0.08*** (0.01)	−0.14*** (0.02)	0.69***	87.7	85.9	160
	17	GAI	−12.7*** (1.6)	177.0** (82.7)	25.2*** (9.9)	0.09*** (0.01)	−0.08*** (0.02)	0.72***	81.3	87.7	130
		ETI ^a	−6.1*** (0.9)	295.6** (121.7)	24.6*** (9.9)	0.08*** (0.01)	−0.1*** (0.02)	0.75***	92.7	83.6	130

Table 5 continued

Microform type	Plot number	GAI/ ETI	P_1	k_1	a_1	b_1	c_1	R^2	F value	RMSE	N
ML	11	GAI ^a	−17.0*** (1.3)	151.6*** (40.5)	31.1*** (8.6)	0.09*** (0.01)	−0.003 ^{NS} (0.01)	0.89***	309.5	55.5	165
		ETI	−6.2*** (1.0)	466.7*** (182.8)	1.1 ^{NS} (1.5)	0.2*** (0.04)	−0.16*** (0.06)	0.83***	195.5	55.5	165
	13	GAI ^a	−14.1*** (1.2)	143.9*** (46.1)	25.4*** (7.5)	0.09*** (0.01)	−0.03*** (0.01)	0.86***	194.1	51.3	136
		ETI	−5.6*** (0.1)	299.1*** (105.0)	11.9** (5.6)	0.09*** (0.01)	−0.06*** (0.02)	0.84***	166.7	54.7	136
	15	GAI ^a	−11.7*** (1.4)	236.4** (98.6)	16.6*** (6.7)	0.07*** (0.01)	−0.12*** (0.02)	0.77***	129.4	67.2	161
		ETI	−6.1*** (1.4)	570.7** (293.1)	7.5* (5.0)	0.07*** (0.01)	−0.17*** (0.04)	0.73***	106.1	72.4	161

ETI or GAI shows the parameters for Eq. 2 (GAI) and Eq. 3 (ETI), respectively. Microform acronyms are explained in Table 1 and text

^{NS} not significant at the 1% level

*, **, *** significant at 10, 5 and 1% level of significance, respectively

^a Indicates which equation was used for modelling the CO₂ flux over the investigation period

Table 6 Respiration model (Eqs. 4 and 5) parameter values (a_2 in $\mu\text{g CO}_2 \text{ m}^{-2} \text{ s}^{-1}$; b_2 in $^\circ\text{C}^{-1}$; c_2 in cm^{-1} ; u in cm ; s in cm) and their standard errors in parentheses, coefficient of determination (R^2), root mean square error (RMSE in $\mu\text{g CO}_2 \text{ m}^{-2} \text{ s}^{-1}$), F value and number of measurements (N) for all plots

Microform type	Plot number	L/A	a_2	b_2	c_2	u	s	R^2	F value	RMSE	N
OHO	1	A ^a	9.6*** (3.2)	0.04*** (0.01)	−0.08*** (0.03)	–	–	0.57***	84.1	20.8	128
		L	7192.7 ^{NS} (297941.1)	0.04*** (0.01)	–	−81.1 ^{NS} (5224.3)	−12.2 ^{NS} (17.)	0.57***	55.6	20.8	128
	4	A ^a	6.0*** (1.6)	0.08*** (0.01)	−0.07*** (0.01)	–	–	0.83***	313.2	17.4	129
		L	26.9*** (8.7)	0.07*** (0.01)	–	10.0*** (3.2)	5.0** (2.4)	0.84***	221.9	16.9	129
OH	2	A	10.6* (6.3)	0.06*** (0.01)	−0.05*** (0.01)	–	–	0.64***	90.9	56.2	106
		L ^a	74.4** (33.6)	0.06*** (0.01)	–	−24.6*** (4.7)	−5.6 ^{NS} (5.3)	0.65***	62.2	55.5	106
	3	A	6.7*** (2.3)	0.07*** (0.01)	0.07*** (0.01)	–	–	0.78***	230.9	25.5	133
		L ^a	40.4*** (9.7)	0.06*** (0.01)	–	−14.9*** (1.2)	−3.4** (1.5)	0.80***	173.1	24.2	133

Table 6 continued

Microform type	Plot number	L/A	a_2	b_2	c_2	u	s	R^2	F value	RMSE	N
OL	5	A	13.9*** (4.6)	0.05*** (0.01)	0.08*** (0.02)	–	–	0.75***	195.7	38.1	132
		L ^a	84.9*** (19.1)	0.04*** (0.01)	–	–12.1*** (1.4)	–3.4** (1.2)	0.78***	152.0	35.8	132
	6	A	13.3*** (5.0)	0.05*** (0.01)	0.08*** (0.02)	–	–	0.76***	190.7	44.0	125
		L ^a	101.7*** (28.8)	0.05*** (0.01)	–	–15.7*** (1.8)	–3.5* (1.8)	0.78***	140.1	42.3	125
CL	7	A ^a	17.3*** (6.9)	0.05*** (0.01)	–0.09*** (0.02)	–	–	0.75***	152.4	53.2	104
		L	311.2 ^{NS} (903.2)	0.05*** (0.01)	–	–25.2 ^{NS} (42.2)	–8.4 ^{NS} (7.6)	0.75***	101.1	53.1	104
	8	A	15.1*** (3.6)	0.07*** (0.01)	–0.05*** (0.01)	–	–	0.82***	301.4	26.2	133
		L ^a	45.6*** (11.0)	0.06*** (0.01)	–	–8.2*** (2.1)	–4.6* (2.5)	0.84***	218.9	25.2	133
	18	A	16.2*** (3.4)	0.07*** (0.01)	–0.06*** (0.01)	–	–	0.88***	398.7	22.7	103
		L ^a	46.2*** (7.3)	0.06*** (0.01)	–	–6.1*** (0.8)	–3.0** (1.2)	0.90***	309.7	21.1	103
MHO	10	A ^a	34.0*** (6.8)	0.004 ^{NS} (0.01)	–0.06*** (0.01)	–	–	0.41***	45.7	20.1	133
		L	92.9 ^{NS} (67.4)	0.002 ^{NS} (0.01)	–	–3.3 ^{NS} (12.7)	–7.6 ^{NS} (6.5)	0.42***	31.1	20.0	133
	14	A ^a	31.6*** (6.0)	0.01 ^{NS} (0.01)	–0.04*** (0.01)	–	–	0.34***	33.3	16.9	134
		L	56.8 ^{NS} (44.1)	0.01 ^{NS} (0.01)	–	3.7 ^{NS} (16.1)	–9.5 ^{NS} (12.3)	0.34***	22.5	16.8	134
	16	A ^a	34.6*** (6.8)	0.02** (0.01)	–0.04*** (0.02)	–	–	0.38***	32.1	17.8	108
		L	5034.6 ^{NS} (3677462.3)	0.02 ^{NS} (0.01)	–	–119.0 ^{NS} (18318.4)	–23.9 ^{NS} (123.1)	0.38***	21.2	17.8	108
MH	9	A	10.0*** (2.5)	0.06*** (0.01)	–0.09*** (0.01)	–	–	0.88***	461.9	29.0	132
		L ^a	75.5*** (16.0)	0.06*** (0.01)	–	–12.5*** (2.0)	–4.1*** (1.4)	0.89***	345.5	27.5	132
	12	A	19.3*** (5.0)	0.05*** (0.01)	–0.07*** (0.01)	–	–	0.81***	287.5	39.6	134
		L ^a	98.2*** (20.2)	0.05*** (0.01)	–	–10.7*** (1.8)	–4.1*** (1.6)	0.83***	209.7	38.0	134
	17	A	26.0*** (5.8)	0.06*** (0.01)	–0.06*** (0.01)	–	–	0.83***	235.3	31.4	102
		L ^a	69.5*** (12.4)	0.05*** (0.01)	–	–4.1*** (1.2)	–3.5** (1.5)	0.84***	175.7	29.9	102

Table 6 continued

Microform type	Plot number	L/A	a_2	b_2	c_2	u	s	R^2	F value	RMSE	N
ML	11	A ^a	26.5*** (3.6)	0.04*** (0.01)	-0.06*** (0.01)	-	-	0.85***	361.5	17.8	134
		L	61.8*** (14.1)	0.04*** (0.01)	-	-0.95 ^{NS} (3.1)	5.9** (2.5)	0.86***	262.8	17.1	134
	13	A ^a	8.8*** (3.2)	0.05*** (0.01)	-0.1*** (0.02)	-	-	0.77***	187.9	27.1	113
		L	76.3*** (29.2)	0.05*** (0.01)	-	-12.2*** (3.7)	-4.3** (1.9)	0.79***	134.6	26.2	113
	15	A ^a	25.5*** (6.2)	0.05*** (0.01)	-0.08*** (0.01)	-	-	0.77***	218.1	39.0	132
		L	105.7** (43.9)	0.05*** (0.01)	-	-7.7 ^{NS} (5.8)	-5.9* (3.2)	0.78***	38.4	150.0	132

A or L shows the parameters for Eq. 4 (L after Larmola et al. 2004) and Eq. 5 (A after Alm et al. 1999), respectively. Microform acronyms are explained in Table 1 and text

^{NS} not significant at the 1% level

*, **, *** significant at 10, 5 and 1% level of significance, respectively

^a Indicates which equation was used for modelling the CO₂ flux over the investigation period

Table 7 GPP model (Eqs. 6 and 7) parameter values (P_2 if modelled based on GAI in $\mu\text{g CO}_2 \text{ m}^{-2} \text{ s}^{-1} \text{ } ^\circ\text{C}^{-1}$, if modelled based on ETI in $\mu\text{g CO}_2 \text{ m}^{-2} \text{ s}^{-1} \text{ } ^\circ\text{C}^{-2}$; k_2 in $\mu\text{mol CO}_2 \text{ m}^{-2} \text{ s}^{-1}$) and their standard errors in parentheses, coefficient of determination (R^2), root mean square error (RMSE in $\mu\text{g CO}_2 \text{ m}^{-2} \text{ s}^{-1}$), F value and number of measurements (N) for all plots

Microform type	Plot number	ETI/ GAI	P_2	k_2	R^2	F value	RMSE	N
OHO	1	GAI ^a	-13.1*** (1.5)	196.8*** (77.3)	0.85***	647.8	36.1	112
		ETI	-2.4*** (0.4)	285.3** (147.2)	0.73***	302.8	48.9	112
	4	GAI	-11.9*** (1.7)	183.4** (91.9)	0.72***	182.7	48.1	117
		ETI ^a	-2.9*** (0.5)	316.1** (128.4)	0.76***	354.4	44.8	117
OH	2	GAI	-13.8*** (3.0)	208.4 ^{NS} (160.0)	0.45***	76.3	73.4	94
		ETI ^a	-3.0*** (0.7)	305.2* (190.0)	0.53***	102.1	68.3	94
	3	GAI	-9.8*** (1.7)	182.9* (115.4)	0.54***	125.8	41.3	110
		ETI ^a	-2.1*** (0.4)	345.8** (166.2)	0.62***	178.4	37.4	110

Table 7 continued

Microform type	Plot number	ETI/ GAI	P_2	k_2	R^2	F value	RMSE	N
OL	5	GAI ^a	-14.0*** (3.1)	419.2* (246.8)	0.64***	183.2	53.5	103
		ETI	-3.9*** (1.5)	705.7 ^{NS} (558.5)	0.37***	58.4	71.4	103
	6	GAI ^a	-11.3*** (1.6)	111.1 ^{NS} (85.2)	0.60***	140.0	63.8	97
		ETI	-3.0*** (0.6)	218.1 ^{NS} (145.9)	0.50***	94.5	71.1	97
CL	7	GAI ^a	-16.0*** (3.0)	206.3* (141.8)	0.65***	160.5	81.4	87
		ETI	-4.3*** (1.0)	328.8* (215.8)	0.60***	125.1	87.9	87
	8	GAI	-45.4 ^{NS} (56.7)	2744.1 ^{NS} (4240.6)	0.14 ^{NS}	21.0	107.3	127
		ETI ^a	-4.4*** (0.9)	380.9** (181.7)	0.61***	198.8	72.0	127
	18	GAI	-7.8*** (1.4)	162.7 ^{NS} (119.9)	0.44***	66.3	82.8	85
		ETI ^a	-3.9*** (0.7)	314.4** (152.3)	0.61***	129.6	69.3	85
MHO	10	GAI ^a	-4.3*** (0.7)	122.9 ^{NS} (86.9)	0.66***	197.6	57.8	106
		ETI	-2.1*** (0.4)	195.9 ^{NS} (123.6)	0.65***	191.2	58.4	106
	14	GAI ^a	-3.7*** (0.5)	155.2** (78.0)	0.80***	471.0	43.4	117
		ETI	-2.2*** (0.4)	203.1* (117.5)	0.71***	278.1	53.0	117
	16	GAI ^a	-3.6*** (0.4)	136.1** (64.3)	0.78***	351.3	36.1	99
		ETI	-1.9*** (0.3)	228.6** (107.8)	0.74***	271.8	39.8	99
MH	9	GAI	-11.6*** (1.8)	201.9* (106.3)	0.64***	209.2	76.9	122
		ETI ^a	-4.0*** (0.6)	268.5** (111.5)	0.72***	302.3	67.9	122
	12	GAI ^a	-9.5*** (1.2)	196.6** (86.7)	0.79***	421.2	61.7	114
		ETI	-4.6*** (0.8)	330.5** (148.6)	0.73***	297.2	70.5	114
	17	GAI	-4.0*** (0.4)	-66.8*** (7.8)	0.25 ^{NS}	27.1	106.9	85
		ETI ^a	-3.2*** (0.4)	152.1* (84.9)	0.68***	176.8	69.7	85

Table 7 continued

Microform type	Plot number	ETI/ GAI	P_2	k_2	R^2	F value	RMSE	N
ML	11	GAI ^a	-13.0*** (1.5)	183.9** (76.9)	0.81***	501.2	82.2	119
		ETI	-5.1*** (0.7)	288.6** (118.4)	0.78***	418.0	88.4	119
	13	GAI	-9.8*** (1.7)	209.1* (127.8)	0.72***	267.1	80.6	104
		ETI ^a	-4.1*** (0.7)	335.6** (167.8)	0.79***	376.4	70.9	104
	15	GAI ^a	-9.0*** (1.3)	217.2** (101.3)	0.81***	471.6	67.1	114
		ETI	-4.9*** (0.9)	355.5** (170.1)	0.76***	358.3	74.8	114

ETI or GAI shows the parameters for Eq. 6 (GAI) and Eq. 7 (ETI), respectively. Microform acronyms are explained in Table 1 and text

NS not significant at the 1% level

*, **, *** significant at 10, 5 and 1% level of significance, respectively

^a Indicates which equation was used for modelling the CO₂ flux over the investigation period

References

- Adamec L (1995) Photosynthetic inorganic carbon use by aquatic carnivorous plants. *Carniv Pl Newslett* 24(2): 50–53
- Alm J, Talanov A, Saarnio S, Silvola J, Ikkonen E, Aaltonen H, Nykänen H, Martikainen PJ (1997) Reconstruction of the carbon balance for microsites in a boreal oligotrophic pine fen, Finland. *Oecologia* 110:423–431
- Alm J, Schulman L, Walden J, Nykänen H, Martikainen PJ, Silvola J (1999) Carbon balance of a boreal bog during a year with an exceptionally dry summer. *Ecology* 80(1): 161–174
- Apps MJ, Kurz WA, Luxmoore RJ, Nilsson LO, Sedjo RA, Schmidt R, Simpson LG, Vinson TS (1993) Boreal forests and tundra. *Water Air Soil Pollut* 70:39–53
- Arneith A, Kurbatova J, Kolle O, Shibistova OB, Lloyd J, Vygodskaya NN, Schulze E-D (2002) Comparative ecosystem-atmosphere exchange of energy and mass in a European Russian and central Siberian bog II. Interseasonal and interannual variability of CO₂ fluxes. *Tellus* 54B: 514–530
- Aurela M, Laurila T, Tuovinen J-P (2002) Annual CO₂ balance of a subarctic fen in northern Europe: importance of the wintertime efflux. *J Geophys Res* 107(D21). doi:10.1029/2002JD002055
- Aurela M, Laurila T, Tuovinen J-P (2004) The timing of snow melt controls the annual CO₂ balance in a subarctic fen. *Geophys Res Lett* 31. doi:10.1029/2004GL020315
- Bubier JL, Frolking S, Crill PM, Linder E (1999) Net ecosystem productivity and its uncertainty in a diverse boreal peatland. *J Geophys Res* 104(D22):27683–27692
- Bubier JL, Crill PM, Mosedale A, Frolking S, Linder E (2003a) Peatland responses to varying interannual moisture conditions as measured by automatic CO₂ chambers. *Glob Biogeochem Cycles* 17(2). doi:10.1029/2002GB001946
- Bubier JL, Bhatia G, Moore TR, Roulet NT, Lafleur PM (2003b) Spatial and temporal variability in growing-season net ecosystem carbon dioxide exchange at a large peatland in Ontario, Canada. *Ecosystems* 6:353–367
- Franzén LG (2006) Increased decomposition of subsurface peat in Swedish raised bogs: are temperate peatlands still net sinks of carbon? *Mires Peat* 1: article 3
- Friborg T, Christensen TR, Sogaard H (1997) Rapid response of greenhouse gas emission to early spring thaw in a subarctic mire as shown by micrometeorological techniques. *Geophys Res Lett* 24(23):3061–3064
- Golovatskaya EA, Dyukarev EA (2009) Carbon budget of oligotrophic mire sites in the southern Taiga of west Siberia. *Plant Soil* 315:19–34
- Gorham E (1991) Northern peatlands: role in the carbon cycle and probable responses to climatic warming. *Ecol Appl* 1:182–195
- Griffis TJ, Rouse WR, Waddington JM (2000) Scaling net ecosystem CO₂ exchange from the community to landscape-level at a subarctic fen. *Glob Change Biol* 6:459–473
- Heikkinen JEP, Virtanen T, Huttunen JT, Elsakov V, Martikainen P (2004) Carbon balance in east European tundra. *Glob Biogeochem Cycles* 18. doi:10.1029/2003GB002054

- Johnson LC, Shaver GR, Giblin AE, Nadelhoffer KJ, Rastetter ER, Laundre JA, Murray GL (1996) Effects of drainage and temperature on carbon balance of tussock tundra microcosms. *Oecologia* 108:737–748
- Kettunen A (2000) Short-term carbon dioxide exchange and environmental factors in a boreal fen. *Verh Internat Verein Limnol* 27:1–5
- Kutzbach L, Wille C, Pfeiffer E-M (2007a) The exchange of carbon dioxide between wet arctic tundra and the atmosphere at the Lena river delta, northern Siberia. *Biogeosciences* 4:869–890
- Kutzbach L, Schneider J, Sachs T, Giebels M, Nykänen H, Shurpali N, Martikainen P, Alm J, Wilmking M (2007b) CO₂ flux determination by closed-chamber methods can be seriously biased by inappropriate application of linear regression. *Biogeosciences* 4:1005–1025
- Laine A, Sottocornola M, Kiely G, Byrne KA, Wilson D, Tuittila E-S (2006) Estimating net ecosystem exchange in a patterned ecosystem: example from blanket bog. *Agric For Meteorol* 138:231–243
- Larmola T, Alm J, Jutinen S, Saarnio S, Martikainen PJ, Silvola J (2004) Floods can cause large interannual differences in littoral net ecosystem productivity. *Limnol Oceanogr* 49(5):1896–1906
- Lindroth A, Lund M, Nilsson M, Aurela M, Christensen TR, Laurila T, Rinne J, Riutta T, Sagerfors J, Ström L, Tuovinen J-P, Vesala T (2007) Environmental controls on the CO₂ exchange in north European mires. *Tellus* 59B:812–825
- Moore TR, Bubier JL, Frohling SE, Lafleur PM, Roulet NT (2002) Plant biomass and production and CO₂ exchange in an ombrotrophic bog. *J Ecol* 90:25–36
- Moore TR, Lafleur PM, Poon DMI, Heumann BW, Seaquist JW, Roulet NT (2006) Spring photosynthesis in a cool temperate bog. *Glob Change Biol* 12:2323–2335
- Oechel WC, Hastings SJ, Vourlitis G, Jenkins M, Reichers G, Grulke N (1993) Recent change of arctic tundra ecosystems from a net carbon dioxide sink to a source. *Nature* 361:520–523
- Panikov NS, Dedysh SN (2000) Cold season CH₄ and CO₂ emission from boreal peat bogs (west Siberia): winter fluxes and thaw activation dynamics. *Glob Biogeochem Cycles* 14(4):1071–1080
- Riutta T, Laine J, Aurela M, Rinne J, Vesala T, Laurila T, Haapanala S, Pihlatie M, Tuittila E-S (2007a) Spatial variation in plant community functions regulates carbon gas dynamics in a boreal fen ecosystem. *Tellus* 59B: 838–852
- Riutta T, Laine J, Tuittila E-S (2007b) Sensitivity of CO₂ exchange of fen ecosystem components to water level variation. *Ecosystems* 10:718–733
- RWS (2009) Russia's Weather Server: http://meteo.infospace.ru/wcarch/html/e_day_stn.sht?num=518. Accessed 30 June 2010
- Sagerfors J, Lindroth A, Grelle A, Klemendtsen L, Weslien P, Nilsson M (2008) Annual CO₂ exchange between nutrient-poor, minerotrophic, boreal mire and the atmosphere. *J Geophys Res* 113. doi:10.1029/2006JG000306
- Schneider J, Kutzbach L, Schulz S, Wilmking M (2009) The closed chamber method overestimates CO₂ respiration fluxes in low-turbulence nighttime conditions. *J Geophys Res* 114. doi:10.1029/2008JG000909
- Schreuder CP, Rouse WR, Griffis TJ, Boudreau LD, Blanken PD (1998) Carbon dioxide fluxes in a northern fen during a hot dry summer. *Glob Biogeochem Cycles* 12(4):129–140
- Schulze E-D, Prokuschkin A, Arneith A, Knorre N, Vaganov EA (2002) Net ecosystem productivity and peat accumulation in a Siberian Aapa mire. *Tellus* 54B:531–536
- Shurpali NJ, Verma SB, Kim J (1995) Carbon dioxide exchange in a peatland ecosystem. *J Geophys Res* 100:14319–14326
- Silvola J, Alm J, Ahlholm U, Nykänen H, Martikainen PJ (1996) The contribution of plant roots to CO₂ fluxes from organic soils. *Biol Fertil Soils* 23:126–131
- Valentini R, Dore S, Marchi G, Mollicone D, Panfyorov M, Rebmann C, Kolle O, Schulze E-D (2000) Carbon and water exchanges of two contrasting central Siberia landscape types: regenerating forest and bog. *Funct Ecol* 14:87–96
- Van der Molen MK, van Huissteden J, Parmentier FJW, Petrescu AMR, Dolman AJ, Maximov TC, Kononov AV, Karsanaev SV, Suzdalov DA (2007) The growing season greenhouse gas balance of a continental tundra site in the Indigirka lowlands, NE Siberia. *Biogeosciences* 4:985–1003
- Waddington JM, Roulet NT (1996) Atmosphere-wetland carbon exchanges: scale dependency of CO₂ and CH₄ exchange on the developmental topography of a peatland. *Glob Biogeochem Cycles* 10(2):233–245
- Waddington JM, Roulet NT (2000) Carbon balance of a boreal patterned peatland. *Glob Change Biol* 6:87–98
- Wallen B, Falkengren-Grerup U, Malmer N (1988) Biomass, productivity and relative rate of photosynthesis of Sphagnum at different water levels on a south Swedish peat bog. *Holarct Ecol* 11:70–76
- Willmott CJ (1982) Some comments on the evaluation of model performance. *Bull Am Meteorol Soc* 63:1309–1313
- Wilson D, Alm J, Riutta T, Laine J, Byrne KA, Farrell EP, Tuittila E-S (2007) A high resolution green area index for modelling the seasonal dynamics of CO₂ exchange in peatland vascular plant communities. *Plant Ecol* 190:37–51
- Wolf U (2009) Above- and belowground methane dynamics of a boreal peatland ecosystem of varying vegetation composition during summer in the Republic of Komi, Russia. Master thesis, University of Göttingen
- Yurova A, Wolf A, Sagerfors J, Nilsson M (2007) Variations in net ecosystem exchange of carbon dioxide in a boreal mire: modeling mechanisms linked to water table position. *J Geophys Res* 112. doi:10.1029/2006JG000342
- Zamolodchikov DG, Karelin DV, Ivaschenko AI, Oechel WC, Hastings SJ (2003) CO₂ flux measurements in Russian far east tundra using eddy covariance and closed chamber techniques. *Tellus* 55B:879–892